HHS Public Access

Author manuscript

Sci Transl Med. Author manuscript; available in PMC 2024 December 14.

Published in final edited form as:

Sci Transl Med. 2023 July 05; 15(703): eade7028. doi:10.1126/scitranslmed.ade7028.

Dysregulated IFN-γ signals promote autoimmunity in STAT1 gain-of-function syndrome

Andrea D. Largent[1], **Katharina Lambert**[2], **Kristy Chiang**[1], **Natali Shumlak**[1,8], **Denny Liggitt**[3], **Mohammed Oukka**[4,5], **Troy R. Torgerson**[6], **Jane H. Buckner**[2], **Eric J. Allenspach**[1,4], **David J. Rawlings**[1,4,5], **Shaun W. Jackson**[1,4,7,*]

[1]Seattle Children's Research Institute, Seattle, WA 98101, USA.

[2]Benaroya Research Institute, Seattle, WA 98101, USA.

[3]Department of Comparative Medicine, University of Washington School of Medicine; Seattle, WA 98195, USA.

[4]Department of Pediatrics, University of Washington School of Medicine; Seattle, WA 98195, USA.

[5]Department of Immunology, University of Washington School of Medicine; Seattle, WA 98195, USA.

[6]Allen Institute for Immunology; Seattle, WA 98109, USA.

[7]Department of Laboratory Medicine and Pathology, University of Washington School of Medicine; Seattle, WA 98195, USA.

[8]Present address: Division of Medical Genetics, University of Washington School of Medicine; Seattle, WA 98195, USA.

[*]Corresponding Author: Shaun W. Jackson, MBChB MD, Seattle Children's Research Institute, 1900 9th Avenue, Seattle, WA 98101, shaun.jackson@seattlechildrens.org (S.W.J).

Author contributions:
Conceptualization: ADL, MO, TRR, JHB, EJA, DJR, SWJ
Methodology: MO, DJR, SWJ
Investigation: ADL, KL, KC, NS, DL
Visualization: ADL, SWJ
Funding acquisition: JHB, DJR, SWJ
Project administration: SWJ
Supervision: SWJ
Writing – original draft: ADL, SWJ
Writing – review & editing: ADL, JHB, EJA, DJR, SWJ

Competing interests:
The authors declare the following competing interests. D.L. is an advisor/consultant to the Cystic Fibrosis Foundation Therapeutics Inc., the University of Washington Institute for Translational Medicine Drug and Device Advisory Board, DNARx LLC., Athira Pharma Inc., Kymera Therapeutics Inc., and Sonomotion Inc. T.R.T has had consulting relationships with Takeda, CSL Behring, Grifols, Enzyvant, X4 Pharmaceuticals, Horizon, and Pharming Healthcare, and performed collaborative studies with Incyte and Eli Lilly. J.H.B. is a Scientific Co-Founder and Scientific Advisory Board member of GentiBio, a consultant for Bristol-Myers Squibb and Hotspot Therapeutics, and has past and current research projects sponsored by Amgen, Bristol-Myers Squib, Janssen, Novo Nordisk, and Pfizer. She is a member of the Type 1 Diabetes Trialnet Study Group, a partner of the Allen Institute for Immunology, and a member of the Scientific Advisory Boards for the La Jolla Institute for Allergy and Immunology and BMS Immunology. D.J.R. is Scientific Co-Founder, Scientific Advisor and Scientific Advisory Board member of GentiBio, and Scientific Co-Founder and Scientific Advisory Board member of BeBiopharma Inc. He has past and current funding from GentiBio, CSL-Behring, BeBiopharma Inc., and Emendo Bio for unrelated studies. S.W.J. previously is a consultant for ChemoCentryx, Inc. All other authors declare that they have no competing interests.

Abstract

Heterozygous *STAT1* (signal transducer and activator of transcription 1) gain-of-function (GOF) mutations promote a clinical syndrome of immune dysregulation characterized by recurrent infections and predisposition to humoral autoimmunity. To gain insights into immune characteristics of STAT1-driven inflammation, we performed deep immunophenotyping of pediatric patients with STAT1 GOF syndrome and age-matched controls. Affected individuals exhibited dysregulated $CD4^+$ T cell and B cell activation, including expansion of Th1-skewed C-X-C Motif Chemokine Receptor 3-positive ($CXCR3^+$) populations that correlated with serum autoantibody titers. To dissect underlying immune mechanisms, we generated *Stat1* GOF transgenic mice ($Stat1^{GOF}$ mice) and confirmed the development of spontaneous humoral autoimmunity that recapitulated the human phenotype. Despite clinical resemblance to human regulatory T cell (Treg) deficiency, $Stat1^{GOF}$ mice and humans with STAT1 GOF syndrome exhibited normal Treg development and function. In contrast, STAT1 GOF autoimmunity was characterized by adaptive immune activation driven by dysregulated STAT1-dependent signals downstream of the Type 1 and Type 2 interferon (IFN) receptors. However, in contrast to the prevailing Type 1 IFN-centric model for STAT1 GOF autoimmunity, $Stat1^{GOF}$ mice lacking the type 1 IFN receptor (IFNAR) were only partially protected from STAT1-driven systemic inflammation, whereas loss of Type 2 IFN (IFN-γ) signals abrogated autoimmunity. Lastly, germline *STAT1* GOF alleles are thought to enhance transcriptional activity by increasing total STAT1 protein, but the underlying biochemical mechanisms have not been defined. We showed that IFN-γ receptor deletion normalized total STAT1 expression across immune lineages, highlighting IFN-γ as the critical driver of feedforward STAT1 elevation in STAT1 GOF syndrome.

One Sentence Summary:

Increased type 2 interferon signals, not type 1 interferon activity, drive humoral autoimmunity in STAT1 gain-of-function syndrome.

Introduction:

Human genetic variations resulting in immunodeficiency or the propensity for autoimmunity represent “experiments of nature” that can advance our understanding of the human immune system and may inform the development of targeted therapies for inflammatory disease (1). In 2011, heterozygous gain-of-function (GOF) mutations in *STAT1* (signal transducer and activator of transcription 1) were identified in patients with autosomal dominant chronic mucocutaneous candidiasis (CMCC) (2, 3). Subsequently, the clinical phenotype of STAT1 GOF syndrome was expanded to include systemic autoimmunity, bacterial and viral infections, cerebral aneurysms, and malignancy, in addition to chronic fungal infections (4, 5). Thus, pathogenic GOF mutations in *STAT1* promote a complex syndrome of immune dysregulation, the pathophysiology of which is still poorly understood.

STAT1 GOF syndrome is associated with multiple features of systemic autoimmunity. Among 274 patients in a large international cohort, almost 40% exhibited clinical autoimmunity including autoimmune endocrine diseases (autoimmune thyroiditis or

type 1 diabetes), hematologic autoimmunity (antibody-mediated hemolytic anemia or immune thrombocytopenia), scleroderma and systemic lupus erythematosus (SLE) (5). *STAT1* GOF mutations have also been identified in subjects with immunodysregulation polyendocrinopathy enteropathy X-linked (IPEX)-like syndrome (4, 6). A characteristic feature of STAT1 GOF autoimmunity is development of autoantibody-mediated or -associated diseases. Consistent with this observation, even among patients without clinical autoimmunity, the majority of tested individuals (65%) were positive for autoantibodies, including anti-nuclear and thyroid-specific antibodies (5).

Together, these findings suggest a prominent role for dysregulated B cell activation in the pathogenesis of STAT1 GOF autoimmunity. Crosstalk between autoreactive $CD4^+$ T cells and B cells facilitates the generation of autoantibody-producing plasma cells, via both extra-follicular B cell activation and within spontaneous germinal centers (7). In contrast to the direct association of defective T helper 17 cell (Th17) differentiation with CMCC, the role of altered STAT1 function in humoral autoimmunity is likely complex because STAT1 is expressed in multiple hematopoietic and non-hematopoietic lineages and can be activated downstream of numerous cytokine receptors.

To address the mechanisms underlying STAT1-driven breaks in immune tolerance, we performed multiparameter immunophenotyping of peripheral blood mononuclear cells (PBMCs) from 8 pediatric patients with STAT1 GOF syndrome and 9 age-matched controls. Affected individuals were studied prior to treatment with Janus kinase (JAK) inhibitors, allowing direct insight into the immune landscape of STAT1-driven immune dysregulation. These studies uncovered immune correlates of STAT1 GOF humoral autoimmunity, including expansion of activated CXC motif chemokine receptor 3-positive ($CXCR3^+$) T and B cell populations. In parallel, we generated an inducible knock-in mouse strain allowing lineage-specific expression of the pathogenic $STAT1^{R274Q}$ human mutation. Global $Stat1^{GOF}$ mice developed spontaneous humoral autoimmunity, mirroring the human disease, allowing a detailed interrogation of the cellular and cytokine-specific drivers of STAT1-driven autoimmunity.

Results:

Multiparameter immunophenotyping of pediatric STAT1 GOF syndrome

To gain insight into the immunologic underpinnings of STAT1 GOF syndrome, we used mass cytometry (cytometry by time-of-flight, CyTOF) to phenotype PBMCs from 8 pediatric patients with STAT1 GOF syndrome and 9 age-matched controls. We limited our analyses to pediatric individuals because STAT1 GOF syndrome typically presents in childhood and to minimize the impact of ageing on adaptive immune phenotypes. The genetic and clinical characteristics of the patients with STAT1 GOF syndrome are summarized in Fig. 1A and tables S1 and S2. Initial presentations included recurrent fungal and bacterial infections in most patients, with overt autoimmunity diagnosed in 2 of 8 patients. We first quantified major innate and adaptive immune cell types by manual gating (Fig. S1). Compared with age-matched controls, $CD8^+$ T cells were expanded, whereas the percentage of plasmacytoid dendritic cells (pDCs) was reduced. The proportion of B cells, $CD4^+$ effector T cells, and regulatory T (Treg) cells was similar between patients

and controls. In keeping with previous studies (8), $CD56^{hi}$ natural killer (NK) cells and $CD56^{mid}$ $CD16^{+}$ NK cells were decreased in the peripheral blood in patients with STAT1 GOF syndrome (Fig. 1B).

Despite similar $CD4^{+}$ and $CD8^{+}$ T cell proportions in patients and controls, enhanced STAT1 activity drove broad T cell activation. In keeping with the young age of this cohort, the majority of $CD4^{+}$ and $CD8^{+}$ T cells in controls exhibited a naïve surface phenotype. In contrast, STAT1 GOF syndrome was characterized by a profound loss of naïve $CD4^{+}$ and $CD8^{+}$ T cells, with corresponding increases in effector memory T (TEM), central memory T (TCM), and terminally differentiated effector memory T cell (TEMRA) populations (Fig. 1, C and D). As predicted by the established link with CMCC, patients with STAT1 GOF syndrome exhibited reduced $CXCR3^{-}$ $CCR6^{+}$ Th17 cells within the non-naïve $CD4^{+}$ T cell compartment (Fig. 1E). In addition, we observed an expansion of $CD38^{+}HLA\text{-}DR^{+}$ T cells in affected individuals, with up to 50% of non-naïve $CD8^{+}$ T cells co-expressing CD38 and HLA-DR, findings mirroring the polyclonal T cell activation and CD38 and HLA-DR upregulation characteristic of severe viral infections, including Ebola, influenza, and SARS-CoV-2 infections (9–11). Although the magnitude of $CD38^{+}HLA\text{-}DR^{+}$ T cell expansion varied among patients with STAT1 GOF syndrome, relative $CD4^{+}$ and $CD8^{+}$ T cell activation was tightly correlated (Fig. 1, F to H).

Given the central role for dysregulated T cell:B cell crosstalk in the pathogenesis of humoral autoimmunity, we expanded our analyses within the $CD4^{+}$ T cell and $CD19^{+}$ B cell compartments. Although we observed no change in $PD\text{-}1^{+}CXCR5^{+}$ circulating T follicular helper (cTfh) cells, patients with STAT1 GOF syndrome exhibited an increase in activated $CD38^{+}ICOS^{+}$ cTfh, thought to reflect more recent antigen engagement within GCs (Fig. 1, I, and J) (12, 13). Moreover, cTfhs in STAT1 GOF syndrome were qualitatively remodeled, manifested by increased pro-inflammatory T helper 1 (Th1)/Th17-like cTfh, a trend towards increased Th1-like cells, and the reciprocal differentiation away from Th17-like surface phenotype (Fig. 1K), in keeping with previous reports (14). To aid exploration of this multiparameter dataset, we created a composite sample of concatenated $CD4^{+}$ effector T cells (3500 cells/subject) including 27 T cell surface markers. A t-distributed stochastic neighbor embedding (tSNE) representation of the data highlighted key differences between patients with STAT1 GOF syndrome and controls (Fig. 2A). Enhanced STAT1 activity drove a prominent increase in regions of the tSNE map characterized by high expression of CD45RO, CXCR3, HLA-DR, PD-1, CD95, and CD138 (Fig. 2B). To further delineate the differences between patients with STAT1 GOF syndrome and controls, we used the Phenograph algorithm (15) to identify 9 clusters defined by differential marker expression (Fig. 2, C and D; hereafter T cell clusters T.1 through T.9). Clusters T.2 and T.3 expressed naïve T cell markers CD45RA, CD62L, and CD27 and were predictably reduced in STAT1 GOF syndrome relative to controls. In contrast, patients with STAT1 GOF syndrome exhibited a marked expansion in clusters T.5, T.8, and T.9 (Fig. 2E). Cluster T.5 included activated Th1-like cTfh phenotype cells expressing CXCR5, PD-1, ICOS, CD95, HLA-DR, and the chemokine receptor CXCR3. Clusters T.8 and T.9 likely represented dysregulated $CD4^{+}$ memory T cells expressing high CD24, chemokine receptors CXCR3 and CCR6 (corresponding to Th1/Th17 phenotype), and the heparan-sulfate proteoglycan family molecule CD138 (syndecan 1). Although the functional significance of human $CD138^{+}$

T cells remains to be determined, CD138-expressing memory $CD4^+$ T cells promote disease progression in murine lupus (16), suggesting a potential link with autoimmune pathogenesis. Collectively, these multidimensional analyses highlight distinct subpopulations of $CD4^+$ effector T cells expanded in STAT1 GOF syndrome.

Dysregulated B cell activation in STAT1 GOF syndrome

We next examined the phenotype of B cells in patients with STAT1 GOF syndrome. Despite increased risk for humoral autoimmunity in this disorder, we observed no expansion of circulating $CD27^+CD38^+$ plasmablasts, and both non-switched (NSWM) and switched memory (SWM) B cells were decreased in patients with STAT1 GOF syndrome (in keeping with previous studies (5, 14)) (Fig. 3A). Moreover, we observed no accumulation of lupus-associated B cell populations, such as "activated naïve" (aNAV) and IgD^-CD27^- double negative DN2 B cells (17–19) (Fig. S2). To explore potential unknown B cell subpopulations contributing to STAT1-driven humoral autoimmunity, we projected concatenated $CD19^+$ B cells into the high-dimensional tSNE space using a subset of CyTOF surface markers expressed by human B cells (20). As predicted, samples from patients with STAT1 GOF syndrome exhibited reduced density in tSNE regions corresponding with switched and unswitched memory B cells ($CD27^{hi}IgD^{lo}IgM^{lo}$ and $CD27^{hi}IgD^+IgM^+$). In parallel, there was a marked STAT1-driven expansion in tSNE regions characterized by retained IgM and IgD expression, reduced CD19 and CXCR5 abundance, and upregulation of CXCR3 and CD138 (Fig. 3, B and C). Phenograph clustering identified 12 unique B cell clusters within the dataset (denoted as B.1 through B.12). Consistent with these findings, controls exhibited an increase in clusters B.2 and B.5, corresponding to IgM^+CD27^+ NSWM and IgM^-CD27^+ SWM B cells, respectively. In contrast, *STAT1* GOF syndrome was characterized by expansion of clusters B.4, B.7, and B.9, which each retained variable IgD and IgM and colocalized within the tSNE space. These clusters were characterized by reduced CD19/CD21 expression and downregulation of the chemokine receptor CXCR5, required for B cell follicular migration (21), predicted to reflect STAT1-driven B cell activation via an extrafollicular pathway. Although reminiscent of $CD21^{lo}$ B cells expanded in human SLE (18, 19), these populations lacked expression of CD11c and CD95. Cluster B.7 exhibited marked upregulation of Th1-lineage chemokine receptor CXCR3 and the plasma cell marker CD138, suggesting that these cells may be antibody-secreting cell (ASC) precursors (Fig. 3, D to F). We then developed a manual gating strategy to assess for phenotypic changes within the IgD^+CD27^- B cell compartment and confirmed expansion of $CXCR5^{lo}CXCR3^+$ B cells in STAT1 GOF syndrome (Fig. 3, G and H). In summary, STAT1 GOF syndrome is characterized by dysregulated B cell activation and expansion of IgM^+ B cells downregulating the follicular homing receptor CXCR5 and upregulating the Th1-defining marker CXCR3.

Correlation between STAT1 GOF lymphocyte phenotype and increased serum autoantibodies

Cellular crosstalk between autoreactive $CD19^+$ B cell and $CD4^+$ T cells facilitates humoral autoimmunity. For this reason, we performed a correlation analysis on $CD4^+$ T cell and B cell Phenograph clusters, focusing on those subpopulations exhibiting statistically significant differences between patients with STAT1 GOF syndrome and controls ($P<0.05$ by two-tailed

Mann-Whitney test). Across the combined samples, the proportion of naïve and activated B and T cell subsets was tightly correlated (Fig. 4A). When we limited these analyses to patients with STAT1 GOF syndrome, we noted that increases in B cell cluster B.7 ($CD138^{hi}CXCR5^{lo}CXCR3^{hi}$) were associated with an expansion in Th1-like cTfh cells (T.5; $CXCR3^{hi}CXCR5^{hi}PD\text{-}1^{hi}ICOS^{hi}$) and the activated memory $CD4^+$ T cell cluster T.9 ($CD45RA^{lo}CD45RO^{hi}CD38^{mid}HLA\text{-}DR^{hi}CXCR5^{mid}CXCR3^{hi}$) (Fig. 4B). Although future studies are needed to define the antigenic targets of these populations, the parallel expansion of $CXCR5^+$ cTfh-like cells and activated B cells suggests a role for $CD4^+$ T cell help in facilitating STAT1-dependent B cell responses.

Next, we examined whether STAT1-driven adaptive immune activation correlated with serum autoantibody titers. Among patients with STAT1 GOF syndrome, the extent of $CD4^+$ T cell and $CD19^+$ B cell activation varied markedly. Thus, to gain an unbiased assessment of this variability, we used principal components analysis [PCA; using ClustVis (22)] to compare the immune profiles of controls and patients with STAT1 GOF syndrome based on relative representation of Phenograph clusters (Fig. 4C). As predicted, affected patients clearly separated from controls, although STAT1 GOF samples were more dispersed in PCA space, with patients SCH04, SCH05, and to a lesser extent SCH06 exhibiting greater separation from healthy controls. SCH04 and SCH05 were among the three individuals diagnosed with clinical autoimmunity or noted to have high-titer autoantibodies on diagnostic testing (table S1). We examined the breadth of the serum autoantibody repertoire using a microarray panel consisting of 128 disease-associated autoantigens. This analysis was performed for each of the 9 age-matched controls, on serial serum samples from patients with STAT1 GOF syndrome, and for 3 additional patients with SLE as positive controls (Fig. 4D). The patients with SLE exhibited minimal IgM autoreactivity, but exhibited high-titer IgG autoantibodies binding RNA-associated specificities, including the U1 small nuclear ribonucleoprotein complex (U1-snRNP-A, U1-snRNP-BB', U1-snRNP-C, U1-snRNP-68/70). In contrast with this relatively focused autoantibody repertoire in SLE, patients with STAT1 GOF syndrome exhibited widespread IgM and IgG autoantibodies targeting diverse disease-associated autoantigens. For example, patient SCH04 produced high-titer IgM and IgG autoantibodies binding single-stranded (ssDNA) and double-stranded DNA (dsDNA). The IgG autoantibody repertoire in patient SCH06 targeted diverse autoantigens, including liver kidney microsomal type 1 antibody (LKM1), Factor H, the muscarinic receptor, insulin, and histone components. Despite a prominent expansion of $CXCR5^{lo}CXCR3^+$ B cells, patient SCH05 lacked both IgM and IgG autoantibodies at the time of immunophenotyping sample collection. However, 12 months later SCH05 developed high-titer anti-dsDNA IgM, suggesting that phenotypic features of STAT1-driven immune dysregulation may portend future breaks in immune tolerance. In summary, STAT1 GOF syndrome is characterized by polyclonal IgM and IgG autoreactivity targeting diverse disease-associated specificities. Although limited patient numbers preclude definitive conclusions, the development of immune dysregulation appears to correlate with serum autoantibodies in STAT1 GOF syndrome.

Generation and validation of *Stat1* GOF knock-in model

To further delineate the immune mechanisms underlying STAT1 GOF syndrome, we generated a inducible knock-in mouse model allowing *Cre*-mediated conditional expression of the pathogenic $Stat1^{R274Q}$ mutation [recurrently identified in 33 patients from 16 independent kindreds (5)] within the endogenous *Stat1* gene; a knock-in strategy that leads to endogenous regulation of *Stat1* expression in all relevant lineages following *Cre*-expression. The design and genetic validation of this model is shown in Fig. S3. We first crossed $Stat1^{R274Q}$ transgenic mice with the ubiquitous CMV-Cre strain (23) to induce global expression of the $Stat1^{R274Q}$ allele in all cellular lineages (hereafter designated $Stat1^{GOF}$). As predicted, ex vivo type 2 interferon (IFN-γ) stimulation induced a $Stat1^{GOF}$ gene dose-dependent increase in STAT1 phosphorylation (pSTAT1) in $CD4^+$ T cells and $CD19^+$ B cells, confirming that $Stat1^{R274Q}$ functions as a GOF variant in mice (Fig. 5, A and B). Human studies have indicated that *STAT1* GOF mutations enhance STAT1 transcriptional activity by either delaying STAT1 dephosphorylation (24, 25) or by increasing total STAT1 protein expression (26–29). In keeping with the latter model, total STAT1 protein was increased in $Stat1^{GOF}$ mice, whereas STAT1 dephosphorylation (as defined by the rate of pSTAT1 decline as a percentage of peak phospho-STAT1) was unaffected (Fig. 5, C to E). During Th1 differentiation, STAT1 induces expression of the lineage-defining transcription factor T-bet, which cements Th1 differentiation and promotes secretion of the canonical cytokine IFN-γ (30). In keeping with this role for STAT1 in regulating Th1 vs. Th17 differentiation, we observed an expansion of splenic Th1 cells and reciprocal decrease in enteric Th17 cells in $Stat1^{GOF}$ animals (Fig. S3). Thus, the $Stat1^{GOF}$ transgenic mouse strain exhibits enhanced STAT1 activity and models the functional impact of human *STAT1* GOF mutations.

Spontaneous humoral autoimmunity in $Stat1^{GOF}$ mice

To test whether *STAT1* GOF promotes breaks in immune tolerance, we aged cohorts of heterozygous $Stat1^{WT/GOF}$ and homozygous $Stat1^{GOF/GOF}$ mice and littermate controls. By 6 months of age, $Stat1^{GOF}$ animals developed Hep-2 anti-nuclear antibodies (ANA) as well as anti- dsDNA and anti-Sm/RNP autoantibodies, with this increase most apparent in homozygous $Stat1^{GOF/GOF}$ mice (Fig. 5, F to H). Serum autoantibodies were skewed towards the T-bet-dependent IgG2c subclass, which has been linked to autoimmune pathogenesis via complement fixation and activation of myeloid Fc-receptors (31, 32). Assessment of the broader autoantibody repertoire using an autoantigen microarray demonstrated that the $Stat1^{GOF}$ allele drove widespread IgG and IgG2c reactivity across a broad spectrum of disease-associated autoantigens (Fig. 5I; Fig. S4).

Autoreactive plasma cells can be generated within spontaneous GCs or via extra-follicular B cell activation pathways, with multiple STAT1-dependent cytokines including type 1 IFN, IL-6, IL-21, IL-27, and IFN-γ, facilitating breaks in B cell tolerance (33–42). Consistent with this model, $Stat1^{GOF}$ mice exhibited gene dose-dependent splenic enlargement and spontaneous GC formation, as evidenced by flow cytometry quantification of PNA^+FAS^+ GC B cells and $CXCR5^+PD\text{-}1^+$ Tfh cells (Fig. 5, J to L). The $Stat1^{GOF}$ allele also drove expansion of $CD11b^+CD11c^+$ age- and autoimmunity-associated B cells (ABCs) (Fig. 5M), a memory B cell population derived following extra-follicular B cell activation (43).

Stat1^{GOF} mice also exhibited increased splenic and bone marrow TACI^{+}IRF4^{+} plasma cells, presumably comprised of extra-follicular-derived short-lived plasmablasts and GC-derived long-lived populations, respectively (44, 45) (Fig. 5, N and O).

Tfh differentiation is driven by the master regulator BCL-6, which reciprocally represses T-bet and Th1-lineage differentiation (46, 47). Based on this model, enhanced STAT1-dependent T-bet might be predicted to limit Tfh differentiation. However, although Th1 and Tfh cells are functionally distinct lineages, they share a developmental link and neither subset fully represses T-bet or BCL-6, respectively (48, 49). A subset of Tfh cells are known to produce IFN-γ during a GC response (48, 50), and T-bet expression early in Tfh differentiation has been shown to epigenetically alter mature Tfhs and allow for ongoing IFN-γ production (51). In keeping with this model, *Stat1*^{GOF} animals exhibited a gene dose-dependent increase in T-bet expression in Tfh cells (Fig 5, P and Q), mirroring the expansion of “Th1-like” activated cTfh in the human patients (Fig. 1G).

Although initially identified in T cells, T-bet also exerts multiple independent impacts on B cell function. These include promotion of IgG2a/c class-switch recombination (32, 52), maintenance of IgG2a/c^{+} memory B cell survival (53), and B cell migration via the induction of surface CXCR3 expression (54, 55). The *Stat1*^{GOF} allele drove a step-wise increase in T-bet expression in CD11c^{+}CD11b^{+} ABCs, and to a lesser extent in GC B cells (Fig 5, P and Q). Thus, in addition to promoting overall Tfh, GC B cell, and ABC expansion, enhanced STAT1 activity alters the phenotype of activated B and T cells in *Stat1*^{GOF} mice by promoting cell-intrinsic T-bet expression.

Lastly, we assessed whether *Stat1*^{GOF} mice manifest systemic inflammation reminiscent of clinical autoimmunity in human *STAT1* GOF syndrome. Analysis of renal disease uncovered prominent glomerular immune complex deposits comprising IgG2c and complement C3 in homozygous *Stat1*$^{GOF/GOF}$ mice. In keeping with IgG2c subclass antibodies driving autoimmune inflammation, histopathology revealed active *Stat1*$^{GOF/GOF}$ glomerulonephritis manifested by mesangial expansion and glomerular hypercellularity (Fig. 6, A and B). Given the diverse autoimmune manifestations of human STAT1 GOF syndrome, we performed a detailed histopathological assessment for organ inflammation, focusing on wild-type (WT) versus homozygous *Stat1*$^{GOF/GOF}$ mice. *Stat1*$^{GOF/GOF}$ animals exhibited widespread inflammatory lesions in the lung, liver, salivary gland, and pancreas, comprised of dense accumulations of small lymphoid cells, minimal histiocytes and plasma cells, and rare neutrophils (Fig. 6, C to F). Together these observations demonstrated that endogenously-regulated expression of a common *STAT1* GOF variant is sufficient to drive humoral autoimmunity within the non-autoimmune prone C57BL/6 background; findings that highlight the critical importance of regulated STAT1 signaling in maintenance of immune tolerance.

Normal Treg development and function in STAT1 GOF syndrome

The clinical similarity between STAT1 GOF and IPEX syndromes (4, 6) has suggested that altered Treg function might mediate STAT1 GOF-driven autoimmunity. However, in keeping with previous reports (4), the proportion of CD127^{lo}CD25^{hi} Treg was equivalent in STAT1 GOF patients and age-matched controls (Fig. S5). Increased STAT1 signals also did not

alter the proportion of CXCR5$^+$ T follicular regulatory (Tfr) cells, required to limit humoral autoimmunity (56), in patients with STAT1 GOF syndrome (Fig. S5).

To further address this question, we examined Treg development, surface phenotype, and suppressor function in *Stat1^{GOF}* mice. The number and proportion of splenic CD25$^+$Foxp3$^+$ Tregs were similar in WT, *Stat1$^{WT/GOF}$*, and *Stat1$^{GOF/GOF}$* mice (Fig. 6G). Increased STAT1 activity did not impact CTLA-4, Helios, or CD25 expression on Tregs (Fig. S5). *Stat1$^{GOF/GOF}$* Treg exhibited normal or possibly slightly increased in vitro suppressive activity, suggesting that Treg dysfunction is not a major driver of autoimmunity in STAT1 GOF syndrome (Fig. 6, H and I).

However, as ex vivo functional assays do not fully recapitulate in vivo Treg biology, we directly examined whether Treg-intrinsic *Stat1^{GOF}* expression results in loss of immune tolerance. We crossed “unflipped” (non-Cre-affected) *Stat1^{GOF}* mice with *Foxp3$^{YFP/Cre}$* animals (57) and confirmed efficient *Stat1^{GOF}* recombination in *Foxp3^{YFP+}* Treg (Fig. S5). Similar to global *Stat1^{GOF}* animals, male *Foxp3$^{YFP/Cre}$.Stat1$^{WT/GOF}$* animals exhibited normal YFP$^+$ Treg numbers in spleen and lymph nodes (LN), relative to *Foxp3$^{YFP/Cre}$.Stat1$^{WT/WT}$* controls (Fig. 6J). In addition, Foxp3-driven *Stat1^{GOF}* expression did not alter Treg CD25, CTLA-4, or Helios expression (Fig. 6, K and L). Lastly, aged *Foxp3$^{YFP/Cre}$.Stat1$^{WT/GOF}$* mice lacked features of immune activation and humoral autoimmunity observed in global *Stat1^{GOF}* animals, including no expansion of Tfh cells, GC B cells, ABCs, or plasma cells (Fig. S5). Thus, although these findings do not preclude more subtle defects in Treg function, our combined human and murine data suggest a limited role for altered Treg biology in STAT1 GOF autoimmunity.

Dysregulated type 2 interferon signaling and autoimmunity in STAT1 GOF syndrome

Type 1 IFN-induced STAT1 phosphorylation results in the formation of IFN-stimulated gene factor 3 (ISGF3) complex comprising IFN-regulatory protein 9 (IRF9) and STAT1/STAT2 heterodimers. In contrast, IFN-γ signals induce phospho-STAT1 homodimers termed gamma-interferon activation factor (GAF). ISGF3 and GAF subsequently translocate to the nucleus and regulate gene transcription by binding interferon-stimulated response elements (ISRE) and gamma-interferon-activated sites (GAS), respectively (58). While the prevailing model holds that enhanced type 1 IFN activity underlies autoimmunity in STAT1 GOF syndrome (5, 58), IFN-γ receptors are critical for initial breaks in immune tolerance in murine models (33–35). Human STAT1 GOF CD4$^+$ T cells and CD19$^+$ B cells exhibited increased pSTAT1 in response to both type 1 IFN (IFN-α and IFN-β) and IFN-γ stimulation (Fig. 7A), implicating either IFN family in autoimmunity in STAT1 GOF syndrome.

For this reason, we intercrossed *Stat1$^{GOF/GOF}$* animals with mice lacking either type 1 IFN [IFNAR; *Ifnar$^{-/-}$* (59)] or type 2 IFN [IFN-γR; *Ifngr$^{-/-}$* (60)] receptors. Whereas IFN-γR deletion abrogated STAT1-driven autoantibodies, a similar proportion of *Ifnar$^{-/-}$.Stat1$^{GOF/GOF}$* and *Ifnar$^{+/+}$.Stat1$^{GOF/GOF}$* animals developed class-switched anti-dsDNA and anti-Sm/RNP titers (Fig. 7B). Moreover, STAT1-driven immune activation was abolished in *Ifngr$^{-/-}$.Stat1$^{GOF/GOF}$* mice, as evidenced by reduced spleen size and loss of expanded Tfh cell, GC B cell, and ABC populations. In contrast, loss of type 1 IFN signals only partially ameliorated T and B cell activation in *Stat1$^{GOF/GOF}$* mice ((Fig.

7, C to E). These differential roles for type 1 versus type 2 IFN in driving breaks in immune tolerance extended to analyses of systemic inflammation. Although reduced compared with IFNAR-sufficient *Stat1*$^{GOF/GOF}$ controls, we observed ongoing organ low-grade inflammation in *Ifnar*$^{-/-}$.*Stat1*$^{GOF/GOF}$ mice. In contrast, IFN-γR deletion eliminated histopathologic evidence of STAT1-dependent systemic inflammation (Fig. 7, F and G).

Lastly, we examined whether loss of type 1 or type 2 IFN signals impacted the relative increase in T-bet and total STAT1 expression in *Stat1*^{GOF} animals. IFN-γR deletion prevented *Stat1*^{GOF}-driven increase in T-bet expression by activated Tfh cells, GC B cells, and ABCs, and restored total STAT1 expression to that of WT controls (Fig. 8, A and B). In contrast, loss of type 1 IFN signals only partially ameliorated these STAT1-dependent changes. Because STAT1 activation induces its own transcription (61), these data implicate enhanced IFN-γ signals as a central driver of increased total STAT1 protein in STAT1 GOF syndrome. To test this idea, we stimulated WT and *Stat1*$^{GOF/GOF}$ B cells in vitro on feeder cell lines expressing CD40-ligand (CD40L) and B-cell activating factor (BAFF) (62), together with increasing concentrations of IFN-γ. In addition to elevated basal STAT1 concentrations, *Stat1*$^{GOF/GOF}$ B cells exhibited proportionally greater IFN-γ-driven increases in total STAT1 (Fig. 8C). These findings lend support to a model in which an altered threshold of IFN-γ signals promotes STAT1 GOF pathogenesis via a feedforward mechanism, findings which may account for the characteristic clinical heterogeneity of the human disease. Consistent with this model, total STAT1 expression in B and T cell lineages of patients with STAT1 GOF syndrome correlated with the proportion of activated B and T cell clusters in each patient (Fig. 8D). In addition, B cell STAT1 expression correlated with the proportion of manually-gated IgD^{+}CD27^{-}CXCR5^{lo}CXCR3^{+} B cells (Fig. 8E). Relative to CXCR5^{hi} B cells, total STAT1 was increased in CXCR5^{lo} B cells in both controls and patients with STAT1 GOF syndrome, implicating STAT1-dependent signals in the genesis of this B subset (Fig. 8F).

Discussion

The study of rare genetic variants resulting in immune dysregulation has informed our understanding of human biology. However, the identification and functional characterization of specific mutations linked with human immune dysfunction represent only the first steps in delineating disease-specific mechanisms underlying individual syndromes. Here, we combined multiparameter immunophenotyping of human STAT1 GOF syndrome with a detailed characterization of *Stat1*^{GOF} knock-in mice to interrogate the biology of STAT1-driven immune dysregulation. Patients with STAT1 GOF syndrome, including those with and without clinical autoimmunity or active infection, exhibited profound alterations in the CD4^{+} and CD8^{+} T cell compartments, with loss of naïve T cells and expansion of activated memory subsets. Of specific relevance to humoral autoimmunity was the STAT1-driven increase in Th1-skewed CXCR3^{+} activated cTfh cells, which may provide T cell help to autoreactive B cells. Although patients with STAT1 GOF syndrome manifested no increase in CD27^{+} switched and unswitched memory B cells or lupus-associated aNAV or DN2 B cells (17–19), the increase in CXCR3^{+} cTfh was accompanied by a parallel expansion of CXCR3^{+}IgD^{+}IgM^{+} B cells characterized by downregulation of the follicular homing

receptor CXCR5, implicating extra-follicular B cell activation in the pathogenesis of STAT1-driven humoral autoimmunity.

Although these data highlight immune correlates of autoimmunity in STAT1 GOF syndrome, limited access to human samples and the confounding effects of recurrent infection prevented definitive conclusions as to causation. For this reason, we generated an inducible *Stat1*^{GOF} knock-in model which exhibited similar spontaneous immune activation and systemic autoimmunity on a non-autoimmune genetic background raised in specific pathogen free conditions. This model also afforded new insights into the cellular and cytokine-specific drivers of breaks in immune tolerance. Contrary to previous speculation, we observed no evidence for Treg dysfunction as a cause for STAT1 GOF autoimmunity. In addition, we show that IFN-γ receptor activation, and not type 1 IFN activity, is required for STAT1-dependent breaks in immune tolerance.

During the pathogenesis of humoral autoimmunity, autoreactive B cells recognizing self-ligands act as antigen-presenting cells, presenting autoantigens to cognate CD4$^+$ T cells and providing costimulatory signals and B cell-derived cytokines necessary for Tfh differentiation (33, 43, 63, 64). Subsequently, extrafollicular pre-GC and GC Tfh support the generation of pathogenic plasma cells via parallel extrafollicular and GC B cell activation pathways. Although defined by their ability to support GC function, the cytokine milieu during early Tfh differentiation impacts the subsequent biology of this lineage. Subpopulations of “Th1-like”, “Th2-like”, and “Th17-like” Tfh develop in response to specific pathogens and thereby tune B cell responses. An important consequence of this model for disease pathogenesis is that the threshold of cytokine signals must be tightly regulated to prevent breaks in immune tolerance.

In this context, the development of humoral autoimmunity in *Stat1*^{GOF} mice was accompanied by increased expression of the Th1-defining transcription factor T-bet in CD4$^+$ Tfh cells, GC B cells, and ABCs, that mirrored the expansion of human cTfh cells and activated B cells expressing the T-bet regulated chemokine receptor CXCR3 (54). Importantly, increased CXCR5^{lo}CXCR3$^+$ B cells in patients with STAT1 GOF syndrome correlated with autoantibody titers, suggesting a link between dysregulated T-bet$^+$ B cells and STAT1-driven humoral autoimmunity. Despite lacking CD11c expression, the surface phenotype of these CXCR3$^+$ B cells in STAT1 GOF syndrome is reminiscent of aNAV or DN B cells expanded in SLE (17–19).

Of the many STAT1-dependent cytokine receptors, enhanced type 1 IFN signaling has been linked to the autoimmunity seen in STAT1 GOF syndrome (5), based on the prominent “interferon gene signature” in human SLE (65–67). Both STAT1 GOF syndrome and polygenic SLE are characterized by ANA; however, a direct link between increased type 1 IFN and breaks in B cell tolerance has not been established. Patients with genetic “type 1 interferonopathies” (for example, Aicardi Goutières syndrome (AGS) and STING-associated vasculopathy with onset in infancy (SAVI)) frequently lack ANA (68), implicating additional cytokine(s) in initiating breaks in immune tolerance. In this context, independent groups uncovered a critical role for IFN-γR signals in the pathogenesis of murine SLE, via cell-intrinsic impacts on GC B cells (33, 34) and Tfhs (35). Further, we

showed that IFN-γ promotes STAT1-dependent IL-6 production by B cells, a critical step for Tfh differentiation in murine lupus (64). Informed by these data, we directly compared the impact of type 1 versus type 2 IFN receptor deletion on STAT1 GOF autoimmunity. Notably, IFN-γR deletion prevented STAT1-driven breaks in immune tolerance, highlighting a central role for dysregulated IFN-γ signaling in the pathogenesis of autoimmunity associated with STAT1 GOF syndrome. In contrast, loss of type 1 IFN signals modestly reduced systemic inflammation, without impacting autoantibody titers. These findings are consistent with longitudinal clinical data in human SLE, in which increased type 1 IFN activity correlates with onset of symptoms but occurs years after initial development of ANA (69, 70). Importantly, the central role for IFN-γ in the clinical symptoms of STAT1 GOF syndrome may extend to CMCC. Recent data indicates that enhanced STAT1-dependent IFN-γ signaling induces intrinsic defects in skin barrier function, resulting in a favorable local tissue niche for fungal pathogens (71, 72).

In addition to defining the cytokine driver of STAT1-driven tolerance breaks, our study informs the biochemical understanding of STAT1 GOF syndrome. Although *STAT1* GOF alleles were initially proposed to delay STAT1 dephosphorylation (24, 25), more recent studies reported increased total STAT1 expression, but unaffected STAT1 dephosphorylation in patients with STAT1 GOF syndrome (26–29). Consistent with this latter model, total STAT1 protein was increased in both patients with STAT1 GOF syndrome and $Stat1^{R274Q}$ expressing animals. IFN-γR deletion abolished this increase in total STAT1 expression across multiple immune lineages resulting in normalization of STAT1-dependent systemic inflammation. Since STAT1 regulates its own transcription (61), these findings highlight IFN-γ as a critical driver of a feedforward inflammatory cascade in STAT1 GOF syndrome.

Our study has several limitations. STAT1 GOF syndrome is a rare disorder characterized by substantial clinical heterogeneity, with about one third of patients exhibiting autoimmunity in the largest international cohort (5). Given that we had relatively few samples available for immunophenotyping studies, we were unable to assess whether specific immune parameters correlated with STAT1 GOF clinical manifestations or the development of autoimmunity. In addition, the cross-sectional study design limited our ability to establish a causal role for any immune subsets in the pathogenesis of STAT1-driven autoimmunity. Although we hypothesize that $CXCR5^{lo}CXCR3^{+}$ B cells act as a precursor for autoantibody-producing plasma cells, proving this link would require further analyses, such as single-cell B cell receptor sequencing to delineate clonal lineage trees. Alternatively, analysis of longitudinal samples from individual treatment-naïve patients could inform the CyTOF phenotypes linked to breaks in tolerance, but such samples were not available and logistically challenging. Lastly, our animal modeling focused on a single variant lying in the STAT1 coiled-coil domain (CCD). While neither the presence of autoimmunity nor the relative expansion of activated B and T cells correlated with specific mutation types in our dataset, in vitro modeling of separate *STAT1* GOF alleles has uncovered diverse patterns of differential gene expression following IFN-α or IFN-γ stimulation (73–75). For this reason, the current transgenic strain may not inform the phenotype of every pathogenic mutation identified in patients with STAT1 GOF syndrome.

Despite these caveats, our study has important translational implications. For example, hematopoietic stem cell transplantation (HSCT) for STAT1 GOF syndrome is potentially curative, but historical outcomes are poor with secondary graft failure observed in about 50% of subjects (73). We speculate that muti-dimensional CyTOF immunophenotyping of patients with STAT1 GOF syndrome might predict poor outcomes post-HSCT and support the use of targeted biologics for a subset of patients prior to transplant conditioning. In addition, multiple United States Food and Drug Administration (FDA)-approved agents are available that either neutralize cytokine activity or block downstream JAK-STAT signaling. Given the relatively greater importance of dysregulated IFN-γ signaling in STAT1 GOF-associated autoimmunity, our data suggest that directly blocking IFN-γ [emapalumab (74)] or JAK1/JAK2 signals [ruxolitinib (75)], is likely to confer greater benefits in comparison to type 1 IFN-directed therapies under development for the treatment of SLE [anifrolumab (76); selective tyrosine kinase 2 (TYK2) inhibitors (77)]. Moreover, the observation that IFN-γ drives feedforward increases in total STAT1 expression highlights the importance of sustained treatment with the goal of normalizing STAT1 expression and restoring immune tolerance in patients with STAT1 GOF syndrome.

Materials and Methods

Study Design

The aims of this study were to determine the immune alterations in pediatric patients with STAT1 GOF syndrome and to interrogate the underlying cellular mechanisms using an inducible knock-in mouse model allowing lineage-specific expression of the pathogenic *STAT1*^{R274Q} human mutation. We used CyTOF to interrogate PBMCs from 8 individuals with STAT1 GOF syndrome (ages 2–11), and 9 randomly-identified age- and sex-matched healthy controls. Cytokine stimulation of PBMCs was performed in serum-free media for 30 minutes at 37°C with or without cytokines (IFN-α, IFN-β, or INF-γ) and total and phosphorylated STAT1 measured by flow cytometry. Patient sera were submitted for autoantibody microarray analysis by the University of Texas Southwestern Medical Center (UTSW) Microarray Core. Research protocols were approved by the Seattle Children's Research Institute (SCRI) and Benaroya Research Institute (BRI) Institutional Review Boards. Participants or their parents provided written informed consent before participation in the study. All available pediatric STAT1 GOF samples in the Seattle Children's Immunology Biorepository were analyzed and no outliers were excluded. No power calculations were performed. All experiments and data analysis were performed by investigators blinded to sample demographics. Sampling and experimental replicates are specified in the figure legends.

Inducible *Stat1*^{GOF} knock-in murine model:

Stat1^{GOF} knock-in mice were generated at Biocytogen using a targeting strategy designed to allow *Cre*-driven replacement of WT exon 10 with R274Q-expressing mutant exon 10. In frame *Stat1*^{GOF} allele recombination was confirmed using polymerase chain reaction (PCR) and digital droplet PCR (ddPCR) assays. For murine studies, male and female experimental animals and littermate controls were sacrificed at 6 months of age unless

otherwise indicated. Data are representative of at least 2 independent experiments for all animal modeling.

Statistical analysis

P-values were calculated using Prism (Graphpad). Normally distributed data (as determined by D'Agostino test) was analyzed by two-tailed Student's *t* test or the one-way analysis of variance (ANOVA) followed by Tukey's multiple comparison test. Nonparametric data was analyzed using the Mann-Whitney U-test or Kruskal-Wallis test with Dunn's correction. Contingency tables were analyzed using the two-tailed Fischer's exact test. Dots in graphs represent individual human patients or experimental animals. Central horizontal lines in column dot plots display mean values. Boxplots display the median with a central line, the 25^{th} and 75^{th} percentiles with the bottom and top edges of the boxes respectively, and the minimum and maximum values with the whiskers. Statistical details and degree of significance are specified in the figure legends.

Supplementary Material

Refer to Web version on PubMed Central for supplementary material.

Acknowledgments:

The authors gratefully acknowledge the patients and their families for participating in this study. We thank K. Sommer and A. Repele for laboratory management, J. Woods and A. Alsulaimawi for technical assistance, and S. Khim for animal colony management.

Funding:

This work was support by National Institutes of Health grants:

- R03AI139716 (to S.W.J)
- R01AR073938 (to S.W.J)
- R01AR075813 (to S.W.J)
- DP3-DK111802 (to D.J.R)
- R01AI132774 (to J.H.B.)

The content is solely the responsibility of the authors and does not necessarily represent the official views of the NIH.

Additional funding support provided by the:

- Lupus Research Alliance, Novel Research Grant (to S.W.J).
- Seattle Children's Research Institute (SCRI) Center for Immunity and Immunotherapies (CIIT) (to D.J.R and S.W.J)
- SCRI Program for Cell and Gene Therapy (PCGT) (to D.J.R)
- Children's Guild Association Endowed Chair in Pediatric Immunology (to D.J.R)
- Hansen Investigator in Pediatric Innovation Endowment (to D.J.R)
- Benaroya Family Gift Fund (to D.J.R)

Data and materials availability:

All data associated with this study are available in the main text or the supplementary materials.

References:

1. Casanova JL, Abel L, Quintana-Murci L, Immunology taught by human genetics. Cold Spring Harb Symp Quant Biol 78, 157–172 (2013). [PubMed: 24092470]
2. Liu L, Okada S, Kong XF, Kreins AY, Cypowyj S, Abhyankar A, Toubiana J, Itan Y, Audry M, Nitschke P, Masson C, Toth B, Flatot J, Migaud M, Chrabieh M, Kochetkov T, Bolze A, Borghesi A, Toulon A, Hiller J, Eyerich S, Eyerich K, Gulacsy V, Chernyshova L, Chernyshov V, Bondarenko A, Grimaldo RM, Blancas-Galicia L, Beas IM, Roesler J, Magdorf K, Engelhard D, Thumerelle C, Burgel PR, Hoernes M, Drexel B, Seger R, Kusuma T, Jansson AF, Sawalle-Belohradsky J, Belohradsky B, Jouanguy E, Bustamante J, Bue M, Karin N, Wildbaum G, Bodemer C, Lortholary O, Fischer A, Blanche S, Al-Muhsen S, Reichenbach J, Kobayashi M, Rosales FE, Lozano CT, Kilic SS, Oleastro M, Etzioni A, Traidl-Hoffmann C, Renner ED, Abel L, Picard C, Marodi L, Boisson-Dupuis S, Puel A, Casanova JL, Gain-of-function human STAT1 mutations impair IL-17 immunity and underlie chronic mucocutaneous candidiasis. The Journal of experimental medicine 208, 1635–1648 (2011). [PubMed: 21727188]
3. van de Veerdonk FL, Plantinga TS, Hoischen A, Smeekens SP, Joosten LA, Gilissen C, Arts P, Rosentul DC, Carmichael AJ, Smits-van der Graaf CA, Kullberg BJ, van der Meer JW, Lilic D, Veltman JA, Netea MG, STAT1 mutations in autosomal dominant chronic mucocutaneous candidiasis. N Engl J Med 365, 54–61 (2011). [PubMed: 21714643]
4. Uzel G, Sampaio EP, Lawrence MG, Hsu AP, Hackett M, Dorsey MJ, Noel RJ, Verbsky JW, Freeman AF, Janssen E, Bonilla FA, Pechacek J, Chandrasekaran P, Browne SK, Agharahimi A, Gharib AM, Mannurita SC, Yim JJ, Gambineri E, Torgerson T, Tran DQ, Milner JD, Holland SM, Dominant gain-of-function STAT1 mutations in FOXP3 wild-type immune dysregulation-polyendocrinopathy-enteropathy-X-linked-like syndrome. J Allergy Clin Immunol 131, 1611–1623 (2013). [PubMed: 23534974]
5. Toubiana J, Okada S, Hiller J, Oleastro M, Lagos Gomez M, Aldave Becerra JC, Ouachee-Chardin M, Fouyssac F, Girisha KM, Etzioni A, Van Montfrans J, Camcioglu Y, Kerns LA, Belohradsky B, Blanche S, Bousfiha A, Rodriguez-Gallego C, Meyts I, Kisand K, Reichenbach J, Renner ED, Rosenzweig S, Grimbacher B, van de Veerdonk FL, Traidl-Hoffmann C, Picard C, Marodi L, Morio T, Kobayashi M, Lilic D, Milner JD, Holland S, Casanova JL, Puel A, S. G.-o.-F. S. G. International, Heterozygous STAT1 gain-of-function mutations underlie an unexpectedly broad clinical phenotype. Blood 127, 3154–3164 (2016). [PubMed: 27114460]
6. Baxter SK, Walsh T, Casadei S, Eckert MM, Allenspach EJ, Hagin D, Segundo G, Lee MK, Gulsuner S, Shirts BH, Sullivan KE, Keller MD, Torgerson TR, King MC, Molecular diagnosis of childhood immune dysregulation, polyendocrinopathy, and enteropathy, and implications for clinical management. J Allergy Clin Immunol 149, 327–339 (2022). [PubMed: 33864888]
7. Rawlings DJ, Metzler G, Wray-Dutra M, Jackson SW, Altered B cell signalling in autoimmunity. Nat Rev Immunol 17, 421–436 (2017). [PubMed: 28393923]
8. Vargas-Hernandez A, Mace EM, Zimmerman O, Zerbe CS, Freeman AF, Rosenzweig S, Leiding JW, Torgerson T, Altman MC, Schussler E, Cunningham-Rundles C, Chinn IK, Carisey AF, Hanson IC, Rider NL, Holland SM, Orange JS, Forbes LR, Ruxolitinib partially reverses functional natural killer cell deficiency in patients with signal transducer and activator of transcription 1 (STAT1) gain-of-function mutations. J Allergy Clin Immunol 141, 2142–2155 e2145 (2018). [PubMed: 29111217]
9. Mathew D, Giles JR, Baxter AE, Oldridge DA, Greenplate AR, Wu JE, Alanio C, Kuri-Cervantes L, Pampena MB, D'Andrea K, Manne S, Chen Z, Huang YJ, Reilly JP, Weisman AR, Ittner CAG, Kuthuru O, Dougherty J, Nzingha K, Han N, Kim J, Pattekar A, Goodwin EC, Anderson EM, Weirick ME, Gouma S, Arevalo CP, Bolton MJ, Chen F, Lacey SF, Ramage H, Cherry S, Hensley SE, Apostolidis SA, Huang AC, Vella LA, Unit UPCP, Betts MR, Meyer NJ, Wherry

EJ, Deep immune profiling of COVID-19 patients reveals distinct immunotypes with therapeutic implications. Science 369, (2020).

10. Ruibal P, Oestereich L, Ludtke A, Becker-Ziaja B, Wozniak DM, Kerber R, Korva M, Cabeza-Cabrerizo M, Bore JA, Koundouno FR, Duraffour S, Weller R, Thorenz A, Cimini E, Viola D, Agrati C, Repits J, Afrough B, Cowley LA, Ngabo D, Hinzmann J, Mertens M, Vitoriano I, Logue CH, Boettcher JP, Pallasch E, Sachse A, Bah A, Nitzsche K, Kuisma E, Michel J, Holm T, Zekeng EG, Garcia-Dorival I, Wolfel R, Stoecker K, Fleischmann E, Strecker T, Di Caro A, Avsic-Zupanc T, Kurth A, Meschi S, Mely S, Newman E, Bocquin A, Kis Z, Kelterbaum A, Molkenthin P, Carletti F, Portmann J, Wolff S, Castilletti C, Schudt G, Fizet A, Ottowell LJ, Herker E, Jacobs T, Kretschmer B, Severi E, Ouedraogo N, Lago M, Negredo A, Franco L, Anda P, Schmiedel S, Kreuels B, Wichmann D, Addo MM, Lohse AW, De Clerck H, Nanclares C, Jonckheere S, Van Herp M, Sprecher A, Xiaojiang G, Carrington M, Miranda O, Castro CM, Gabriel M, Drury P, Formenty P, Diallo B, Koivogui L, Magassouba N, Carroll MW, Gunther S, Munoz-Fontela C, Unique human immune signature of Ebola virus disease in Guinea. Nature 533, 100–104 (2016). [PubMed: 27147028]
11. Wang Z, Zhu L, Nguyen THO, Wan Y, Sant S, Quiñones-Parra SM, Crawford JC, Eltahla AA, Rizzetto S, Bull RA, Qiu C, Koutsakos M, Clemens EB, Loh L, Chen T, Liu L, Cao P, Ren Y, Kedzierski L, Kotsimbos T, McCaw JM, La Gruta NL, Turner SJ, Cheng AC, Luciani F, Zhang X, Doherty PC, Thomas PG, Xu J, Kedzierska K, Clonally diverse CD38+HLA-DR+CD8+ T cells persist during fatal H7N9 disease. Nature Communications 9, 824 (2018).
12. Herati RS, Reuter MA, Dolfi DV, Mansfield KD, Aung H, Badwan OZ, Kurupati RK, Kannan S, Ertl H, Schmader KE, Betts MR, Canaday DH, Wherry EJ, Circulating CXCR5+PD-1+ response predicts influenza vaccine antibody responses in young adults but not elderly adults. J Immunol 193, 3528–3537 (2014). [PubMed: 25172499]
13. Law H, Mach M, Howe A, Obeid S, Milner B, Carey C, Elfis M, Fsadni B, Ognenovska K, Phan TG, Carey D, Xu Y, Venturi V, Zaunders J, Kelleher AD, Munier CML, Early expansion of CD38+ICOS+ GC Tfh in draining lymph nodes during influenza vaccination immune response. iScience 25, 103656 (2022). [PubMed: 35028536]
14. Ma CS, Wong N, Rao G, Avery DT, Torpy J, Hambridge T, Bustamante J, Okada S, Stoddard JL, Deenick EK, Pelham SJ, Payne K, Boisson-Dupuis S, Puel A, Kobayashi M, Arkwright PD, Kilic SS, El Baghdadi J, Nonoyama S, Minegishi Y, Mahdaviani SA, Mansouri D, Bousfiha A, Blincoe AK, French MA, Hsu P, Campbell DE, Stormon MO, Wong M, Adelstein S, Smart JM, Fulcher DA, Cook MC, Phan TG, Stepensky P, Boztug K, Kansu A, Ikinciogullari A, Baumann U, Beier R, Roscioli T, Ziegler JB, Gray P, Picard C, Grimbacher B, Warnatz K, Holland SM, Casanova JL, Uzel G, Tangye SG, Monogenic mutations differentially affect the quantity and quality of T follicular helper cells in patients with human primary immunodeficiencies. J Allergy Clin Immunol 136, 993–1006 e1001 (2015). [PubMed: 26162572]
15. Levine JH, Simonds EF, Bendall SC, Davis KL, Amir el AD, Tadmor MD, Litvin O, Fienberg HG, Jager A, Zunder ER, Finck R, Gedman AL, Radtke I, Downing JR, Pe'er D, Nolan GP, Data-Driven Phenotypic Dissection of AML Reveals Progenitor-like Cells that Correlate with Prognosis. Cell 162, 184–197 (2015). [PubMed: 26095251]
16. Liu L, Takeda K, Akkoyunlu M, Disease Stage-Specific Pathogenicity of CD138 (Syndecan 1)-Expressing T Cells in Systemic Lupus Erythematosus. Front Immunol 11, 1569 (2020). [PubMed: 32849532]
17. Tipton CM, Fucile CF, Darce J, Chida A, Ichikawa T, Gregoretti I, Schieferl S, Hom J, Jenks S, Feldman RJ, Mehr R, Wei C, Lee FE, Cheung WC, Rosenberg AF, Sanz I, Diversity, cellular origin and autoreactivity of antibody-secreting cell population expansions in acute systemic lupus erythematosus. Nat Immunol 16, 755–765 (2015). [PubMed: 26006014]
18. Wang S, Wang J, Kumar V, Karnell JL, Naiman B, Gross PS, Rahman S, Zerrouki K, Hanna R, Morehouse C, Holoweckyj N, Liu H, Autoimmunity Molecular Medicine T, Manna Z, Goldbach-Mansky R, Hasni S, Siegel R, Sanjuan M, Streicher K, Cancro MP, Kolbeck R, Ettinger R, IL-21 drives expansion and plasma cell differentiation of autoreactive CD11c(hi)T-bet(+) B cells in SLE. Nat Commun 9, 1758 (2018). [PubMed: 29717110]
19. Jenks SA, Cashman KS, Zumaquero E, Marigorta UM, Patel AV, Wang X, Tomar D, Woodruff MC, Simon Z, Bugrovsky R, Blalock EL, Scharer CD, Tipton CM, Wei C, Lim SS, Petri M, Niewold TB, Anolik JH, Gibson G, Lee FE, Boss JM, Lund FE, Sanz I, Distinct Effector B Cells

Induced by Unregulated Toll-like Receptor 7 Contribute to Pathogenic Responses in Systemic Lupus Erythematosus. Immunity 49, 725–739 e726 (2018). [PubMed: 30314758]

20. Glass DR, Tsai AG, Oliveria JP, Hartmann FJ, Kimmey SC, Calderon AA, Borges L, Glass MC, Wagar LE, Davis MM, Bendall SC, An Integrated Multi-omic Single-Cell Atlas of Human B Cell Identity. Immunity 53, 217–232 e215 (2020). [PubMed: 32668225]
21. Forster R, Mattis AE, Kremmer E, Wolf E, Brem G, Lipp M, A putative chemokine receptor, BLR1, directs B cell migration to defined lymphoid organs and specific anatomic compartments of the spleen. Cell 87, 1037–1047 (1996). [PubMed: 8978608]
22. Metsalu T, Vilo J, ClustVis: a web tool for visualizing clustering of multivariate data using Principal Component Analysis and heatmap. Nucleic Acids Res 43, W566–570 (2015). [PubMed: 25969447]
23. Schwenk F, Baron U, Rajewsky K, A cre-transgenic mouse strain for the ubiquitous deletion of loxP-flanked gene segments including deletion in germ cells. Nucleic Acids Res 23, 5080–5081 (1995). [PubMed: 8559668]
24. Hijikata A, Tsuji T, Shionyu M, Shirai T, Decoding disease-causing mechanisms of missense mutations from supramolecular structures. Sci Rep 7, 8541 (2017). [PubMed: 28819267]
25. Fujiki R, Hijikata A, Shirai T, Okada S, Kobayashi M, Ohara O, Molecular mechanism and structural basis of gain-of-function of STAT1 caused by pathogenic R274Q mutation. J Biol Chem 292, 6240–6254 (2017). [PubMed: 28258222]
26. Bernasconi AR, Yancoski J, Villa M, Oleastro MM, Galicchio M, Rossi JG, Increased STAT1 Amounts Correlate with the Phospho-STAT1 Level in STAT1 Gain-of-function Defects. J Clin Immunol 38, 745–747 (2018). [PubMed: 30302727]
27. Weinacht KG, Charbonnier LM, Alroqi F, Plant A, Qiao Q, Wu H, Ma C, Torgerson TR, Rosenzweig SD, Fleisher TA, Notarangelo LD, Hanson IC, Forbes LR, Chatila TA, Ruxolitinib reverses dysregulated T helper cell responses and controls autoimmunity caused by a novel signal transducer and activator of transcription 1 (STAT1) gain-of-function mutation. J Allergy Clin Immunol 139, 1629–1640 e1622 (2017). [PubMed: 28139313]
28. Meesilpavikkai K, Dik WA, Schrijver B, Nagtzaam NM, van Rijswijk A, Driessen GJ, van der Spek PJ, van Hagen PM, Dalm VA, A Novel Heterozygous Mutation in the STAT1 SH2 Domain Causes Chronic Mucocutaneous Candidiasis, Atypically Diverse Infections, Autoimmunity, and Impaired Cytokine Regulation. Front Immunol 8, 274 (2017). [PubMed: 28348565]
29. Zimmerman O, Olbrich P, Freeman AF, Rosen LB, Uzel G, Zerbe CS, Rosenzweig SD, Kuehn HS, Holmes KL, Stephany D, Ding L, Sampaio EP, Hsu AP, Holland SM, STAT1 Gain-of-Function Mutations Cause High Total STAT1 Levels With Normal Dephosphorylation. Front Immunol 10, 1433 (2019). [PubMed: 31354696]
30. Wilson CB, Rowell E, Sekimata M, Epigenetic control of T-helper-cell differentiation. Nature reviews. Immunology 9, 91–105 (2009).
31. Nimmerjahn F, Ravetch JV, Divergent immunoglobulin g subclass activity through selective Fc receptor binding. Science 310, 1510–1512 (2005). [PubMed: 16322460]
32. Peng SL, Szabo SJ, Glimcher LH, T-bet regulates IgG class switching and pathogenic autoantibody production. Proc Natl Acad Sci U S A 99, 5545–5550 (2002). [PubMed: 11960012]
33. Jackson SW, Jacobs HM, Arkatkar T, Dam EM, Scharping NE, Kolhatkar NS, Hou B, Buckner JH, Rawlings DJ, B cell IFN-gamma receptor signaling promotes autoimmune germinal centers via cell-intrinsic induction of BCL-6. The Journal of experimental medicine 213, 733–750 (2016). [PubMed: 27069113]
34. Domeier PP, Chodisetti SB, Soni C, Schell SL, Elias MJ, Wong EB, Cooper TK, Kitamura D, Rahman ZS, IFN-gamma receptor and STAT1 signaling in B cells are central to spontaneous germinal center formation and autoimmunity. The Journal of experimental medicine 213, 715–732 (2016). [PubMed: 27069112]
35. Lee SK, Silva DG, Martin JL, Pratama A, Hu X, Chang PP, Walters G, Vinuesa CG, Interferon-gamma excess leads to pathogenic accumulation of follicular helper T cells and germinal centers. Immunity 37, 880–892 (2012). [PubMed: 23159227]
36. Batten M, Ramamoorthi N, Kljavin NM, Ma CS, Cox JH, Dengler HS, Danilenko DM, Caplazi P, Wong M, Fulcher DA, Cook MC, King C, Tangye SG, de Sauvage FJ, Ghilardi N, IL-27 supports

germinal center function by enhancing IL-21 production and the function of T follicular helper cells. J Exp Med 207, 2895–2906 (2010). [PubMed: 21098093]

37. Vijayan D, Mohd Redzwan N, Avery DT, Wirasinha RC, Brink R, Walters G, Adelstein S, Kobayashi M, Gray P, Elliott M, Wong M, King C, Vinuesa CG, Ghilardi N, Ma CS, Tangye SG, Batten M, IL-27 Directly Enhances Germinal Center B Cell Activity and Potentiates Lupus in Sanroque Mice. J Immunol 197, 3008–3017 (2016). [PubMed: 27619997]
38. Wan CK, Andraski AB, Spolski R, Li P, Kazemian M, Oh J, Samsel L, Swanson PA 2nd, McGavern DB, Sampaio EP, Freeman AF, Milner JD, Holland SM, Leonard WJ, Opposing roles of STAT1 and STAT3 in IL-21 function in CD4+ T cells. Proc Natl Acad Sci U S A 112, 9394–9399 (2015). [PubMed: 26170288]
39. Bubier JA, Sproule TJ, Foreman O, Spolski R, Shaffer DJ, Morse HC 3rd, Leonard WJ, Roopenian DC, A critical role for IL-21 receptor signaling in the pathogenesis of systemic lupus erythematosus in BXSB-Yaa mice. Proc Natl Acad Sci U S A 106, 1518–1523 (2009). [PubMed: 19164519]
40. Jain S, Park G, Sproule TJ, Christianson GJ, Leeth CM, Wang H, Roopenian DC, Morse HC 3rd, Interleukin 6 Accelerates Mortality by Promoting the Progression of the Systemic Lupus Erythematosus-Like Disease of BXSB.Yaa Mice. PloS one 11, e0153059 (2016). [PubMed: 27050763]
41. Arkatkar T, Du SW, Jacobs HM, Dam EM, Hou B, Buckner JH, Rawlings DJ, Jackson SW, B cell-derived IL-6 initiates spontaneous germinal center formation during systemic autoimmunity. J Exp Med 214, 3207–3217 (2017). [PubMed: 28899868]
42. Domeier PP, Chodisetti SB, Schell SL, Kawasawa YI, Fasnacht MJ, Soni C, Rahman ZSM, B-Cell-Intrinsic Type 1 Interferon Signaling Is Crucial for Loss of Tolerance and the Development of Autoreactive B Cells. Cell Rep 24, 406–418 (2018). [PubMed: 29996101]
43. Chiang K, Largent AD, Arkatkar T, Thouvenel CD, Du SW, Shumlak N, Woods J, Li QZ, Liu Y, Hou B, Rawlings DJ, Jackson SW, Cutting Edge: A Threshold of B Cell Costimulatory Signals Is Required for Spontaneous Germinal Center Formation in Autoimmunity. J Immunol 207, 2217–2222 (2021). [PubMed: 34588220]
44. Nutt SL, Hodgkin PD, Tarlinton DM, Corcoran LM, The generation of antibody-secreting plasma cells. Nat Rev Immunol 15, 160–171 (2015). [PubMed: 25698678]
45. Hale M, Rawlings DJ, Jackson SW, The long and the short of it: insights into the cellular source of autoantibodies as revealed by B cell depletion therapy. Curr Opin Immunol 55, 81–88 (2018). [PubMed: 30390507]
46. Nurieva RI, Chung Y, Martinez GJ, Yang XO, Tanaka S, Matskevitch TD, Wang YH, Dong C, Bcl6 mediates the development of T follicular helper cells. Science 325, 1001–1005 (2009). [PubMed: 19628815]
47. Yu D, Rao S, Tsai LM, Lee SK, He Y, Sutcliffe EL, Srivastava M, Linterman M, Zheng L, Simpson N, Ellyard JI, Parish IA, Ma CS, Li QJ, Parish CR, Mackay CR, Vinuesa CG, The transcriptional repressor Bcl-6 directs T follicular helper cell lineage commitment. Immunity 31, 457–468 (2009). [PubMed: 19631565]
48. Lu KT, Kanno Y, Cannons JL, Handon R, Bible P, Elkahloun AG, Anderson SM, Wei L, Sun H, O'Shea JJ, Schwartzberg PL, Functional and epigenetic studies reveal multistep differentiation and plasticity of in vitro-generated and in vivo-derived follicular T helper cells. Immunity 35, 622–632 (2011). [PubMed: 22018472]
49. Nakayamada S, Kanno Y, Takahashi H, Jankovic D, Lu KT, Johnson TA, Sun HW, Vahedi G, Hakim O, Handon R, Schwartzberg PL, Hager GL, O'Shea JJ, Early Th1 cell differentiation is marked by a Tfh cell-like transition. Immunity 35, 919–931 (2011). [PubMed: 22195747]
50. Qi H, T follicular helper cells in space-time. Nature reviews. Immunology 16, 612–625 (2016).
51. Fang D, Cui K, Mao K, Hu G, Li R, Zheng M, Riteau N, Reiner SL, Sher A, Zhao K, Zhu J, Transient T-bet expression functionally specifies a distinct T follicular helper subset. The Journal of experimental medicine 215, 2705–2714 (2018). [PubMed: 30232200]
52. Gerth AJ, Lin L, Peng SL, T-bet regulates T-independent IgG2a class switching. International immunology 15, 937–944 (2003). [PubMed: 12882831]

53. Wang NS, McHeyzer-Williams LJ, Okitsu SL, Burris TP, Reiner SL, McHeyzer-Williams MG, Divergent transcriptional programming of class-specific B cell memory by T-bet and RORalpha. Nature immunology 13, 604–611 (2012). [PubMed: 22561605]
54. Lord GM, Rao RM, Choe H, Sullivan BM, Lichtman AH, Luscinskas FW, Glimcher LH, T-bet is required for optimal proinflammatory CD4+ T-cell trafficking. Blood 106, 3432–3439 (2005). [PubMed: 16014561]
55. Szabo SJ, Kim ST, Costa GL, Zhang X, Fathman CG, Glimcher LH, A novel transcription factor, T-bet, directs Th1 lineage commitment. Cell 100, 655–669 (2000). [PubMed: 10761931]
56. Sage PT, Sharpe AH, T follicular regulatory cells. Immunol Rev 271, 246–259 (2016). [PubMed: 27088919]
57. Rubtsov YP, Rasmussen JP, Chi EY, Fontenot J, Castelli L, Ye X, Treuting P, Siewe L, Roers A, Henderson WR Jr., Muller W, Rudensky AY, Regulatory T cell-derived interleukin-10 limits inflammation at environmental interfaces. Immunity 28, 546–558 (2008). [PubMed: 18387831]
58. Okada S, Asano T, Moriya K, Boisson-Dupuis S, Kobayashi M, Casanova JL, Puel A, Human STAT1 Gain-of-Function Heterozygous Mutations: Chronic Mucocutaneous Candidiasis and Type I Interferonopathy. J Clin Immunol 40, 1065–1081 (2020). [PubMed: 32852681]
59. Muller U, Steinhoff U, Reis LF, Hemmi S, Pavlovic J, Zinkernagel RM, Aguet M, Functional role of type I and type II interferons in antiviral defense. Science 264, 1918–1921 (1994). [PubMed: 8009221]
60. Huang S, Hendriks W, Althage A, Hemmi S, Bluethmann H, Kamijo R, Vilcek J, Zinkernagel RM, Aguet M, Immune response in mice that lack the interferon-gamma receptor. Science 259, 1742–1745 (1993). [PubMed: 8456301]
61. Lehtonen A, Matikainen S, Julkunen I, Interferons up-regulate STAT1, STAT2, and IRF family transcription factor gene expression in human peripheral blood mononuclear cells and macrophages. J Immunol 159, 794–803 (1997). [PubMed: 9218597]
62. Haniuda K, Kitamura D, Induced Germinal Center B Cell Culture System. Bio Protoc 9, e3163 (2019).
63. Giles JR, Kashgarian M, Koni PA, Shlomchik MJ, B Cell-Specific MHC Class II Deletion Reveals Multiple Nonredundant Roles for B Cell Antigen Presentation in Murine Lupus. J Immunol 195, 2571–2579 (2015). [PubMed: 26268653]
64. Arkatkar T, Du SW, Jacobs HM, Dam EM, Hou B, Buckner JH, Rawlings DJ, Jackson SW, B cell-derived IL-6 initiates spontaneous germinal center formation during systemic autoimmunity. The Journal of experimental medicine, (2017).
65. Baechler EC, Batliwalla FM, Karypis G, Gaffney PM, Ortmann WA, Espe KJ, Shark KB, Grande WJ, Hughes KM, Kapur V, Gregersen PK, Behrens TW, Interferon-inducible gene expression signature in peripheral blood cells of patients with severe lupus. Proceedings of the National Academy of Sciences of the United States of America 100, 2610–2615 (2003). [PubMed: 12604793]
66. Bennett L, Palucka AK, Arce E, Cantrell V, Borvak J, Banchereau J, Pascual V, Interferon and granulopoiesis signatures in systemic lupus erythematosus blood. The Journal of experimental medicine 197, 711–723 (2003). [PubMed: 12642603]
67. Kirou KA, Lee C, George S, Louca K, Peterson MG, Crow MK, Activation of the interferon-alpha pathway identifies a subgroup of systemic lupus erythematosus patients with distinct serologic features and active disease. Arthritis and rheumatism 52, 1491–1503 (2005). [PubMed: 15880830]
68. Kim H, Sanchez GA, Goldbach-Mansky R, Insights from Mendelian Interferonopathies: Comparison of CANDLE, SAVI with AGS, Monogenic Lupus. J Mol Med (Berl) 94, 1111–1127 (2016). [PubMed: 27678529]
69. Lu R, Munroe ME, Guthridge JM, Bean KM, Fife DA, Chen H, Slight-Webb SR, Keith MP, Harley JB, James JA, Dysregulation of innate and adaptive serum mediators precedes systemic lupus erythematosus classification and improves prognostic accuracy of autoantibodies. J Autoimmun, (2016).
70. Munroe ME, Lu R, Zhao YD, Fife DA, Robertson JM, Guthridge JM, Niewold TB, Tsokos GC, Keith MP, Harley JB, James JA, Altered type II interferon precedes autoantibody accrual and

elevated type I interferon activity prior to systemic lupus erythematosus classification. Ann Rheum Dis 75, 2014–2021 (2016). [PubMed: 27088255]

71. Niehues H, Rosler B, van der Krieken DA, van Vlijmen-Willems I, Rodijk-Olthuis D, Peppelman M, Schalkwijk J, van den Bogaard EHJ, Zeeuwen P, van de Veerdonk FL, STAT1 gain-of-function compromises skin host defense in the context of IFN-gamma signaling. J Allergy Clin Immunol 143, 1626–1629 e1625 (2019). [PubMed: 30576757]
72. Break TJ, Oikonomou V, Dutzan N, Desai JV, Swidergall M, Freiwald T, Chauss D, Harrison OJ, Alejo J, Williams DW, Pittaluga S, Lee CR, Bouladoux N, Swamydas M, Hoffman KW, Greenwell-Wild T, Bruno VM, Rosen LB, Lwin W, Renteria A, Pontejo SM, Shannon JP, Myles IA, Olbrich P, Ferre EMN, Schmitt M, Martin D, Genomics C. Computational Biology, Barber DL, Solis NV, Notarangelo LD, Serreze DV, Matsumoto M, Hickman HD, Murphy PM, Anderson MS, Lim JK, Holland SM, Filler SG, Afzali B, Belkaid Y, Moutsopoulos NM, Lionakis MS, Aberrant type 1 immunity drives susceptibility to mucosal fungal infections. Science 371, (2021).
73. Leiding JW, Okada S, Hagin D, Abinun M, Shcherbina A, Balashov DN, Kim VHD, Ovadia A, Guthery SL, Pulsipher M, Lilic D, Devlin LA, Christie S, Depner M, Fuchs S, van Royen-Kerkhof A, Lindemans C, Petrovic A, Sullivan KE, Bunin N, Kilic SS, Arpaci F, Calle-Martin O, Martinez-Martinez L, Aldave JC, Kobayashi M, Ohkawa T, Imai K, Iguchi A, Roifman CM, Gennery AR, Slatter M, Ochs HD, Morio T, Torgerson TR, Inborn Errors Working Party of the European Society for B, Marrow T, the Primary Immune Deficiency Treatment C, Hematopoietic stem cell transplantation in patients with gain-of-function signal transducer and activator of transcription 1 mutations. J Allergy Clin Immunol 141, 704–717 e705 (2018). [PubMed: 28601685]
74. Al-Salama ZT, Emapalumab: First Global Approval. Drugs 79, 99–103 (2019). [PubMed: 30623346]
75. Forbes LR, Vogel TP, Cooper MA, Castro-Wagner J, Schussler E, Weinacht KG, Plant AS, Su HC, Allenspach EJ, Slatter M, Abinun M, Lilic D, Cunningham-Rundles C, Eckstein O, Olbrich P, Guillerman RP, Patel NC, Demirdag YY, Zerbe C, Freeman AF, Holland SM, Szabolcs P, Gennery A, Torgerson TR, Milner JD, Leiding JW, Jakinibs for the treatment of immune dysregulation in patients with gain-of-function signal transducer and activator of transcription 1 (STAT1) or STAT3 mutations. J Allergy Clin Immunol 142, 1665–1669 (2018). [PubMed: 30092289]
76. Morand EF, Furie R, Tanaka Y, Bruce IN, Askanase AD, Richez C, Bae SC, Brohawn PZ, Pineda L, Berglind A, Tummala R, Investigators T-T, Trial of Anifrolumab in Active Systemic Lupus Erythematosus. N Engl J Med 382, 211–221 (2020). [PubMed: 31851795]
77. Morand E, Pike M, Merrill JT, Van Vollenhoven R, Werth VP, Hobar C, Delev N, Shah V, Sharkey B, Wegman T, Catlett I, Banerjee S, Singhal S, LB0004 EFFICACY AND SAFETY OF DEUCRAVACITINIB, AN ORAL, SELECTIVE, ALLOSTERIC TYK2 INHIBITOR, IN PATIENTS WITH ACTIVE SYSTEMIC LUPUS ERYTHEMATOSUS: A PHASE 2, RANDOMIZED, DOUBLE-BLIND, PLACEBO-CONTROLLED STUDY. Annals of the Rheumatic Diseases 81, 209–209 (2022).

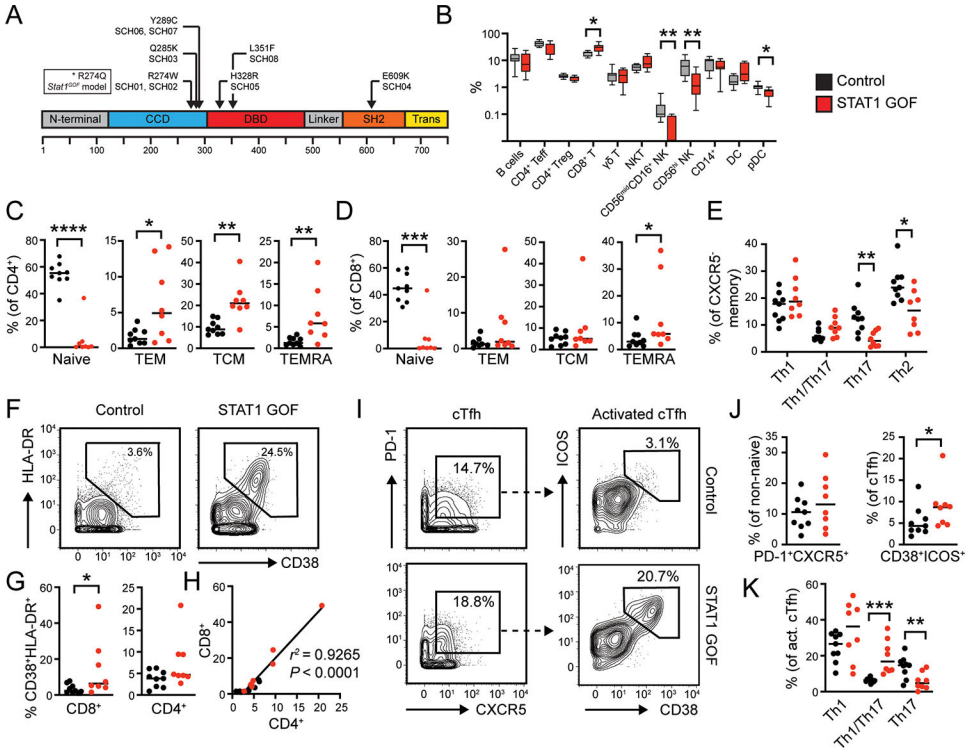

Figure 1: STAT1 GOF immunophenotyping by mass cytometry

(A) Schematic showing location of *STAT1* mutations in the patient cohort. STAT1 protein domains: CCD, Coiled-coil domain; DBD, DNA-binding domain; SH2, Src-Homology 2 domain; Trans, Trans-Activation domain. * Mutation studied in the *Stat1*^{GOF} murine model. (B) Frequencies of major immune cell types amongst total PBMCs. (C and D) Frequencies of naïve, effector memory (TEM), central memory (TCM), terminally differentiated effector memory T cells (TEMRA) as proportion of total CD4$^+$ (C) and CD8$^+$ (D) T cells. (E) Proportion of Th1, Th1/Th17, Th17, and Th2 cells within non-Tfh memory population (CXCR5$^-$CD45RO$^+$CD4$^+$ Teff). (F) Representative flow cytometry plots (gated on non-naïve CD8$^+$) showing expansion of CD38$^+$HLA-DR$^+$ T cells in patients with STAT1 GOF syndrome. Number equals percentage within gate. (G) CD38$^+$HLA-DR$^+$ cells as a percentage of non-naïve CD8$^+$ (left) and CD4$^+$ (right) T cells. (H) CD38$^+$HLA-DR$^+$CD8$^+$ vs. CD38$^+$HLA-DR$^+$CD4$^+$ cells in patients with STAT1 GOF syndrome. Spearman correlation shown. (I) Representative flow cytometry plots showing gating of CXCR5$^+$PD-1$^+$ cTfh and activated CD38$^+$ICOS$^+$ cTfh. Number equals percentage within gate. (J) Percentage of cTfh (left) and percentage of activated cTfh in control and STAT1 GOF syndrome. (K) Percentage of activated cTfh exhibiting Th1, Th1/Th17, and Th17 surface phenotype. (B-K) Each dot represents an individual; black (control), red (STAT1 GOF syndrome). *, P<0.05; **, P<0.01; ***, P<0.001; ****, P<0.0001; by two-tailed Mann-Whitney test. N=1 CyTOF experiment.

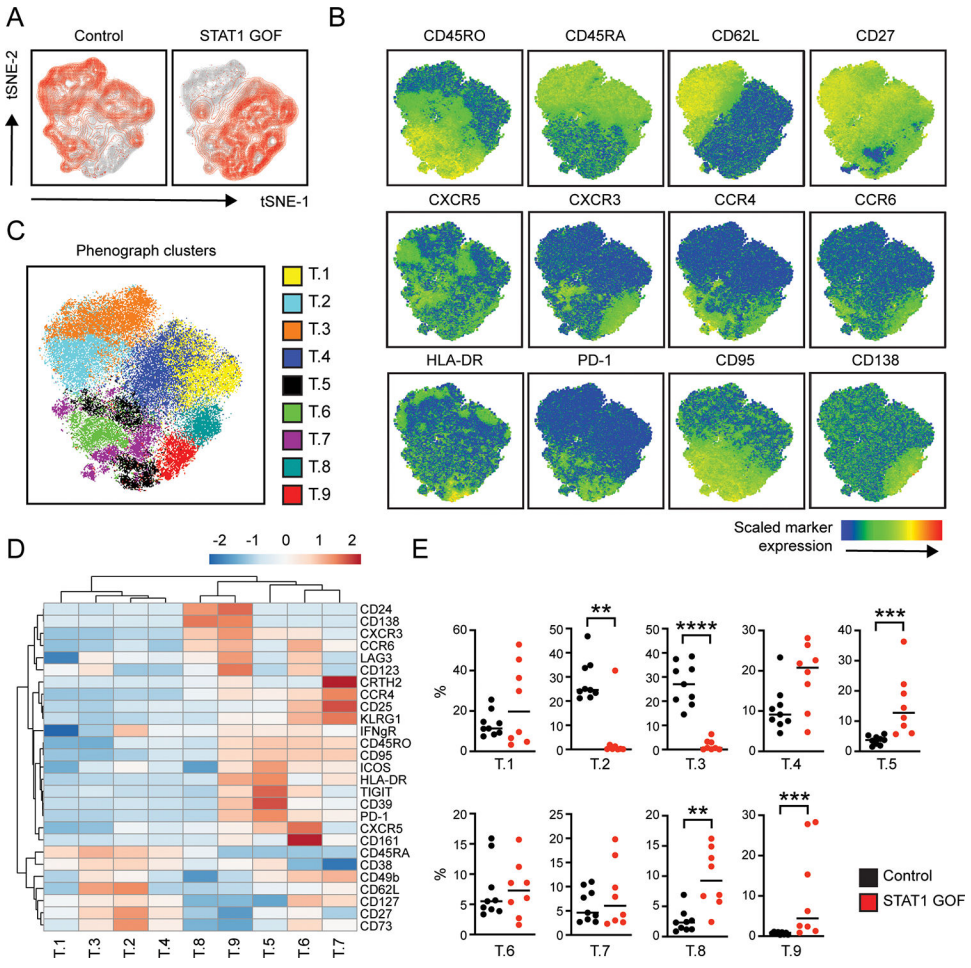

Figure 2: STAT1 GOF syndrome promotes broad changes in the CD4$^+$ T cell compartment

(A) t-SNE projection of effector CD4$^+$ T cell composite sample (3500 representative cells per individual). Red contour plot represents concatenated healthy control (left) and patients with STAT1 GOF syndrome (right). Composite sample including patients and controls shown in grey. (B) Heat maps of select marker expression overlaid on composite t-SNE projection from A. (C) t-SNE projection of CD4$^+$ Teff clusters identified using phenograph. (D) Heatmap of marker MFI in CD4$^+$ Teff phenograph clusters. (E) % of CD4$^+$ Teff cells in each phenograph cluster in controls (black) and patients with STAT1 GOF syndrome (red). **, P<0.01; ***, P<0.001; ****, P<0.0001; by two-tailed Mann-Whitney test. N=1 CyTOF experiment.

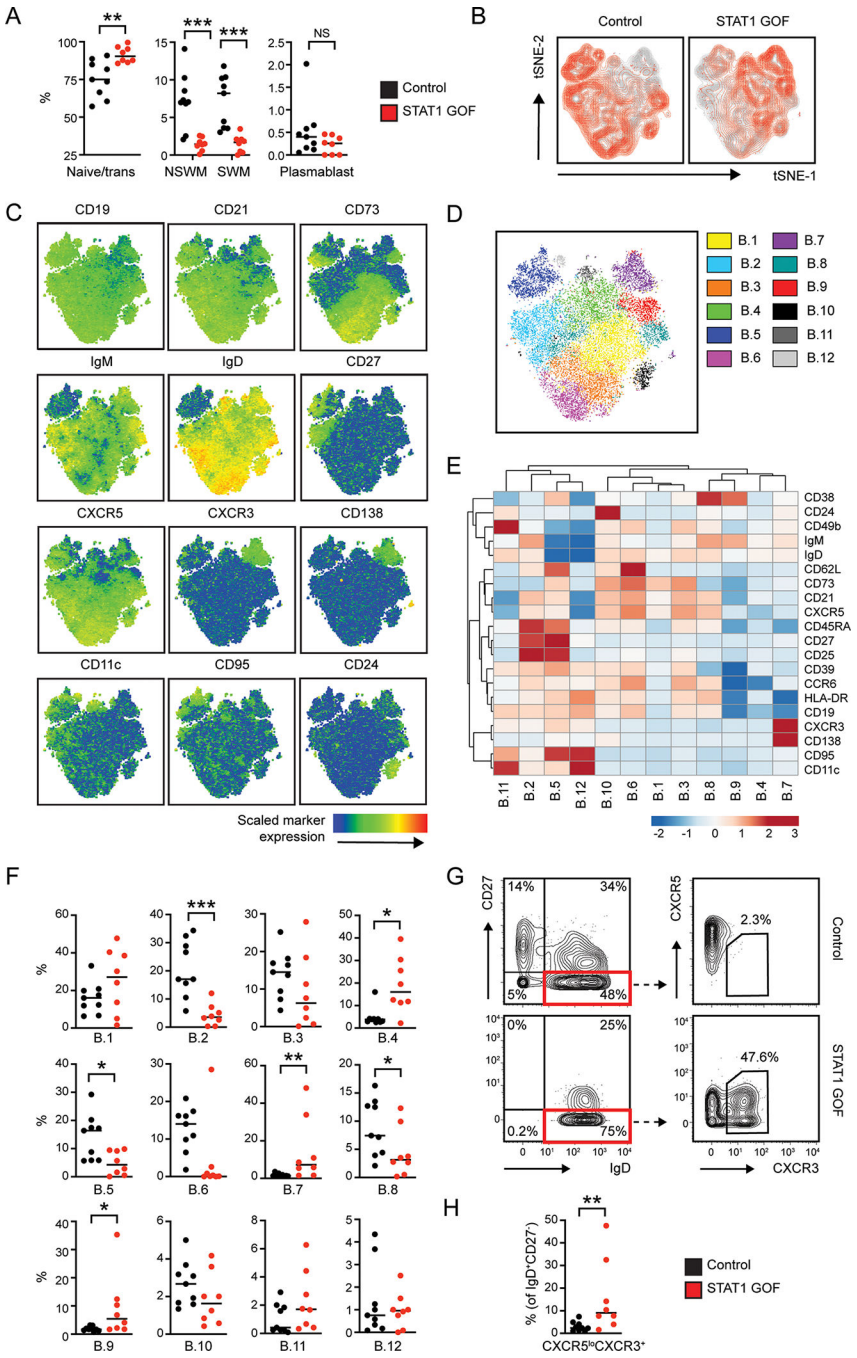

Figure 3: Expansion of activated CXCR3$^+$ B cells in patients with STAT1 GOF syndrome

(A) Percentage of IgD$^+$CD27$^-$ (Naïve/transitional), IgD$^+$CD27$^+$ (NSWM), IgD$^-$CD27$^+$ (SWM), and CD27$^+$CD38$^+$ plasmablasts. (B) t-SNE projection of CD19$^+$ B cell composite sample. Red contour: concatenated control (left) and STAT1 GOF (right). Grey: combined composite sample. (C) Heat maps of select marker expression in composite t-SNE from B. (D) t-SNE projection of CD19$^+$ B cell phenograph clusters. (E) Heatmap of marker MFI in CD19$^+$ B cell phenograph clusters. (F) Percentage of CD19$^+$ B cells in each phenograph cluster. (G) Gating strategy to identify CXCR5^{lo}CXCR3$^+$ subset within IgD$^+$CD27$^-$ B cells.

(H) Percentage of $CXCR5^{lo}CXCR3^{+}$ B cells (of $IgD^{+}CD27^{-}$ gate). (A, F, H) Each point indicates an individual; Control (black) and STAT1 GOF (red). *, $P<0.05$; **, $P<0.01$; ***, $P<0.001$, n.s. not significant; by two-tailed Mann-Whitney test. $N=1$ CyTOF experiment.

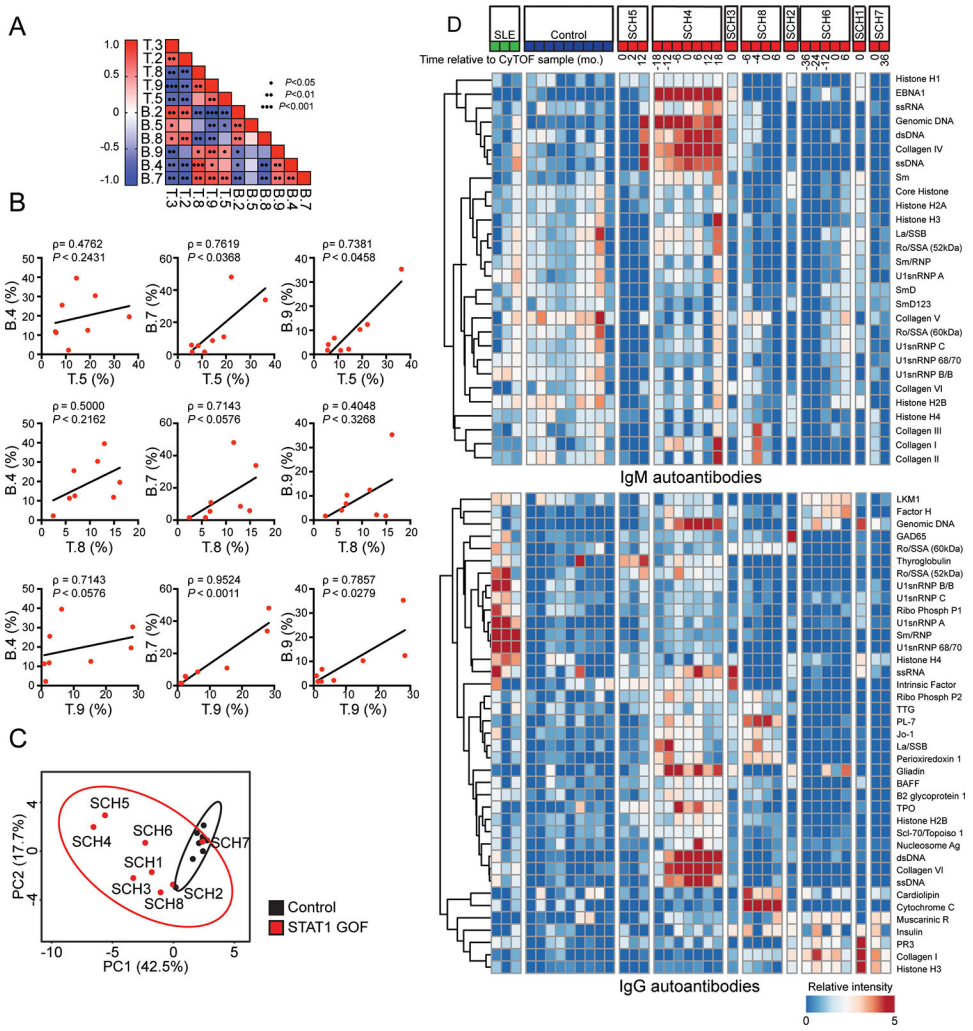

Figure 4: STAT1-driven changes in CD4$^+$ T cell and B cell compartments correlate with autoantibody titers in patients with STAT1 GOF syndrome

(A) Correlation between CD4$^+$ Teff and CD19$^+$ B cell phenograph clusters in control and STAT1 GOF patients. Heat map shows Spearman's rank correlation coefficient. *, P<0.05; **, P<0.01; ***, P<0.001; False-discovery rate correction by Benjamini-Hochberg procedure (<0.05 significance threshold). (B) Spearman correlation of STAT1 GOF CD4$^+$ Teff versus CD19$^+$ B cell phenograph clusters. (C) PCA of CD4$^+$ Teff and CD19$^+$ B cell phenograph cluster distribution in controls (black) versus patients with STAT1 GOF syndrome (red). Ellipses indicate 95% probability range for each group. (D) Heatmap of IgM (upper panel) and IgG (lower panel) autoantibody titers in controls (blue), patients with STAT1 GOF syndrome (red), and patients with SLE (green). Timing of serum collection, relative to CyTOF sample, indicated in months. N=1 CyTOF and autoantibody microarray experiment.

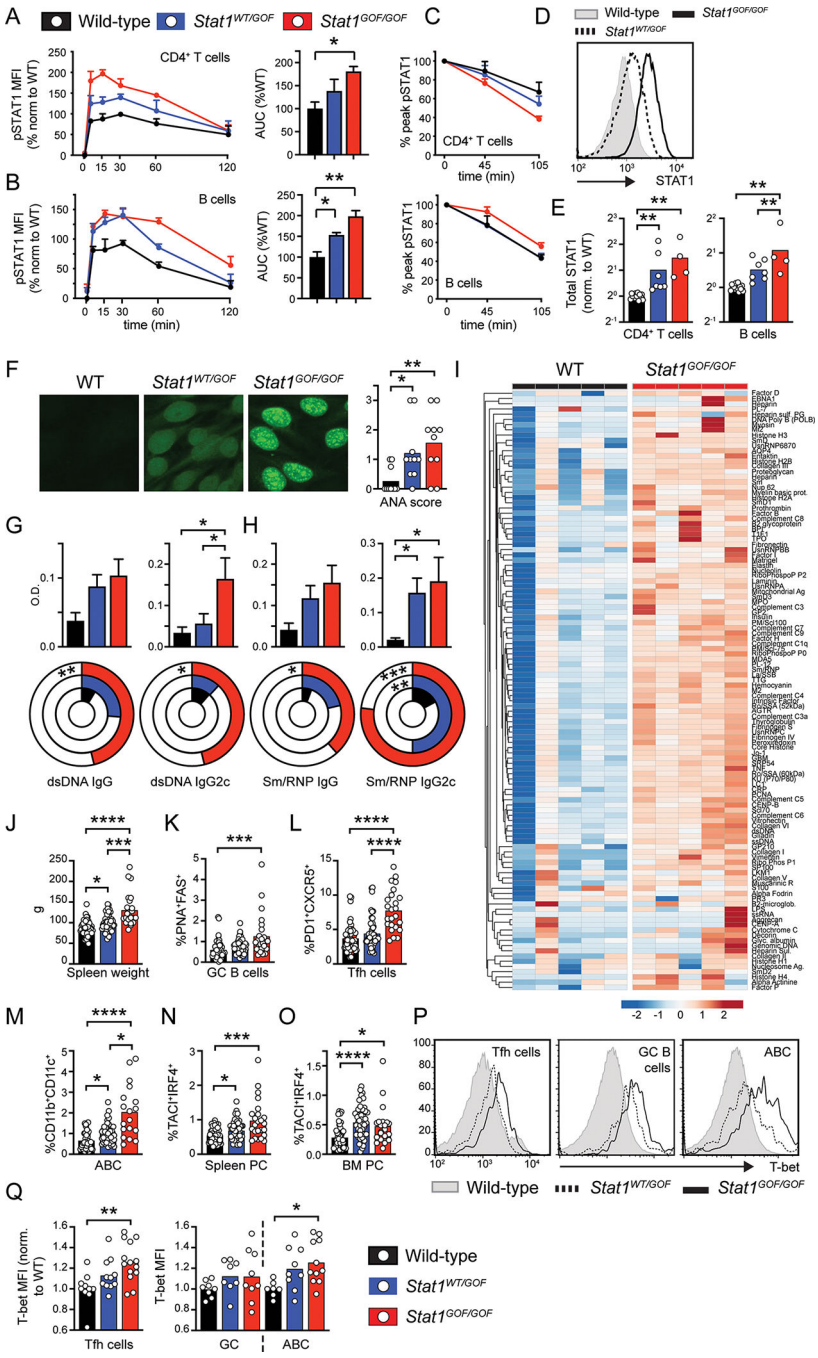

Figure 5: Enhanced STAT1 activity promotes spontaneous humoral autoimmunity in *Stat1*^{GOF} mice

(A and B) IFN-γ-induced phospho-STAT1 (pSTAT1) in naïve CD44^{lo}CD4^{+} T cells (A) and CD19^{+} B cells (B) from WT (black), heterozygous *Stat1*$^{WT/GOF}$ (blue), and homozygous *Stat1*$^{GOF/GOF}$ (red) mice. Right panel: Relative pSTAT1 expression over time, normalized to the peak WT response. Left panel: Quantification of pSTAT1 area under the curve (AUC; normalized to WT). (C) pSTAT1 expression over time expressed as a percentage of peak expression for each respective genotype. (D) Histogram of total STAT1 in CD4^{+} T cells. (E) Total STAT1 MFI (normalized to WT) in indicated subsets. (F) Representative Hep-2 ANA

staining (left) and quantification of ANA intensity (right). (G and H) Anti-dsDNA (G) and anti-Sm/RNP (H) IgG and IgG2c autoAb in animals of indicated genotypes. Top panels: Graph of mean autoAb titer (Error bars indicate SEM*; $P<0.05$, by one-way ANOVA). Lower panel: Pie chart showing percent of animals that are autoAb positive (defined as O.D. > WT mean plus 1 SD) for each antigen/subclass. *, $P<0.05$; **, $P<0.01$; ***, $P<0.001$, by Fisher's exact test relative to WT control. (I) Heatmaps of IgG2c autoantibodies in WT and *Stat1*$^{GOF/GOF}$ mice. Each column represents an independent animal. (J to O) Spleen weight (J), %PNA^{+}FAS^{+} GC B cells (K), %PD1^{+}CXCR5^{+} Tfh cells (L), %CD11b^{+}CD11c^{+} ABCs (M), and %TACI^{+}IRF4^{+} plasma cells in spleen (N) and bone marrow (O) in WT (black), heterozygous *Stat1*$^{WT/GOF}$ (blue), and homozygous *Stat1*$^{GOF/GOF}$ (red) mice. (P) Representative histogram T-bet expression in indicated immune subsets. (Q) T-bet MFI (normalized to WT for each population) in indicated genotype. (A to C) Data representative of 4 independent experiments. Error bars indicate SEM; *, $P<0.05$; **, $P<0.01$, by one-way ANOVA relative to WT control. (E-Q) Each point equals individual animal. *, $P<0.05$; **, $P<0.01$;***, $P<0.001$; ****, $P<0.0001$, by Kruskal-Wallis test with Dunn’s multiple comparison test (E, J to Q) or by one-way ANOVA (F). Data compiled from 4–10 independent mouse cohorts.

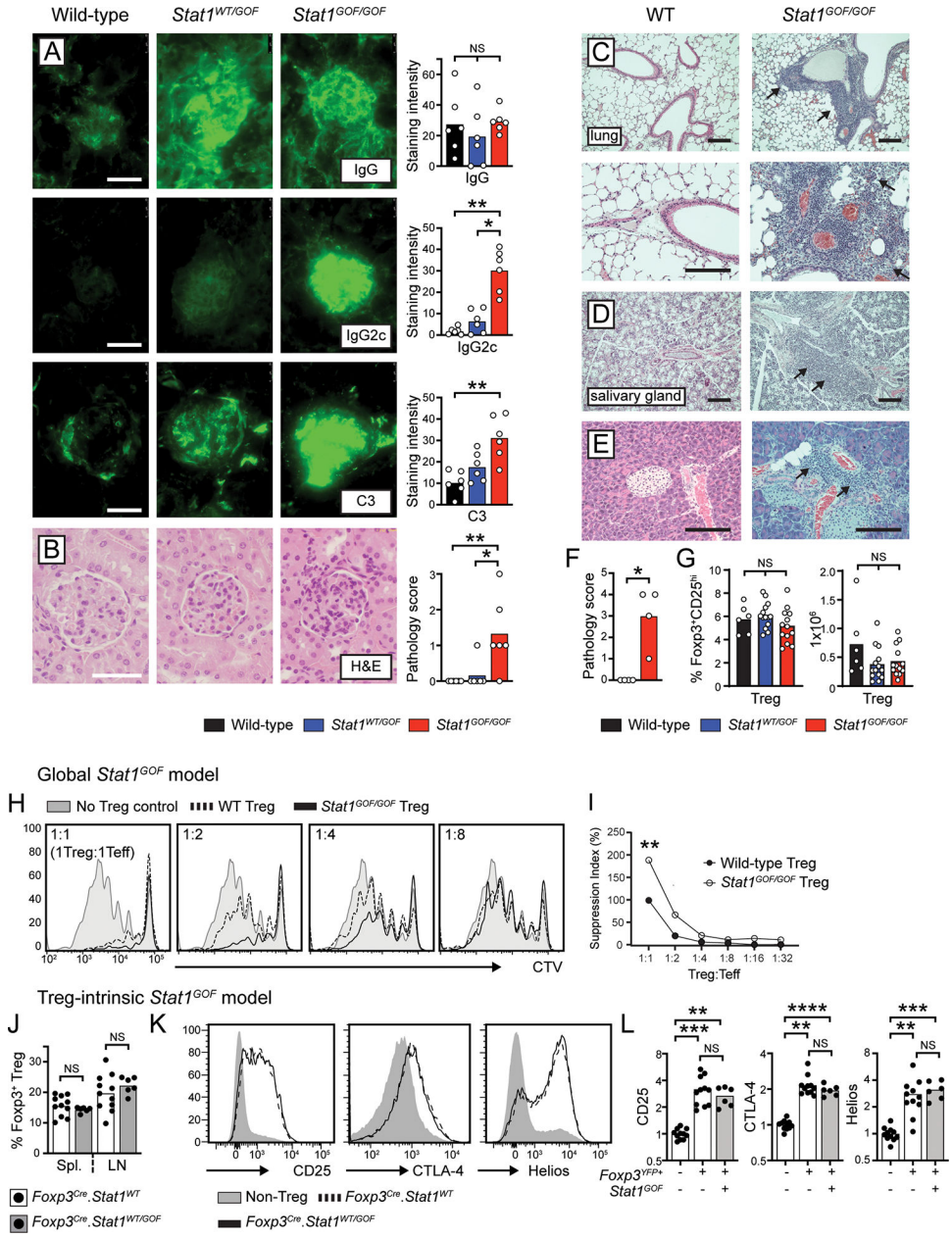

Figure 6: Systemic autoimmunity despite normal regulatory T cell development and function in murine and human STAT1 GOF syndrome

(A) Immunofluorescence (IF) staining for glomerular IgG, IgG2c, and complement C3. Left panels: Representative images. Right panels: Quantification of glomerular IF staining. (B) Representative hematoxylin and eosin (H&E)-stained kidney sections (left) and glomerular inflammation (right; scored from 0–3 based on mesangial expansion and cellularity, glomerular basement membrane (GBM) thickening, and glomerular hypercellularity). (C to E) Representative images showing widespread organ inflammation in homozygous *Stat1*$^{GOF/GOF}$ mice, including: lymphoid cell infiltrates in lungs surrounding pulmonary blood vessels (C; upper panels 10x; arrows) with extension into surrounding airspace resulting in patchy alveolar collapse (lower panels 20x; arrows); and inflammatory cell

accumulations in perivascular and periductal regions of *Stat1*$^{GOF/GOF}$ salivary glands (D; 10x) and pancreas (E; 20x). Bars equal 100μm. (F) Composite score of organ inflammation in *Stat1*^{GOF} model. (G) Percentage (left) and total number (right) of splenic Foxp3^{+}CD25^{+} global WT, *Stat1*$^{WT/GOF}$, and *Stat1*$^{GOF/GOF}$ mice. (H) WT CD4^{+} T cell proliferation by cell-trace violet (CTV) dilution co-cultured with indicated ratios of WT or *Stat1*$^{GOF/GOF}$ Treg. (I) Treg suppression index at different Treg ratios. **, P<0.01, unpaired Student *t* test. (J) Percentage of YFP^{+} Treg in spleen and LN of *Foxp3*^{cre}.*Stat1*$^{WT/WT}$ and *Foxp3*^{cre}.*Stat1*$^{WT/GOF}$ mice. (K) Treg surface marker expression in LN Treg from *Foxp3*^{cre}.*Stat1*$^{WT/WT}$ (dashed line) versus *Foxp3*^{cre}.*Stat1*$^{WT/GOF}$ (solid line) mice. Gray histogram: WT Foxp3^{-}CD4^{+} non-Treg. (L) CD25, CTLA-4, and Helios MFI on CD4^{+} non-Treg vs. Foxp3.YFP^{+} Treg (normalized to WT non-Treg). (A-L) Data representative of 8 independent cohorts with each circle indicating an individual animal. *, P<0.05; **, P<0.01, ***, P<0.001; ****, P<0.0001; ns, not significant, by Kruskal-Wallis test with Dunn's multiple comparison test (A, B, G, L), and two-tailed Mann-Whitney test (F, J). Bars equal 50μm.

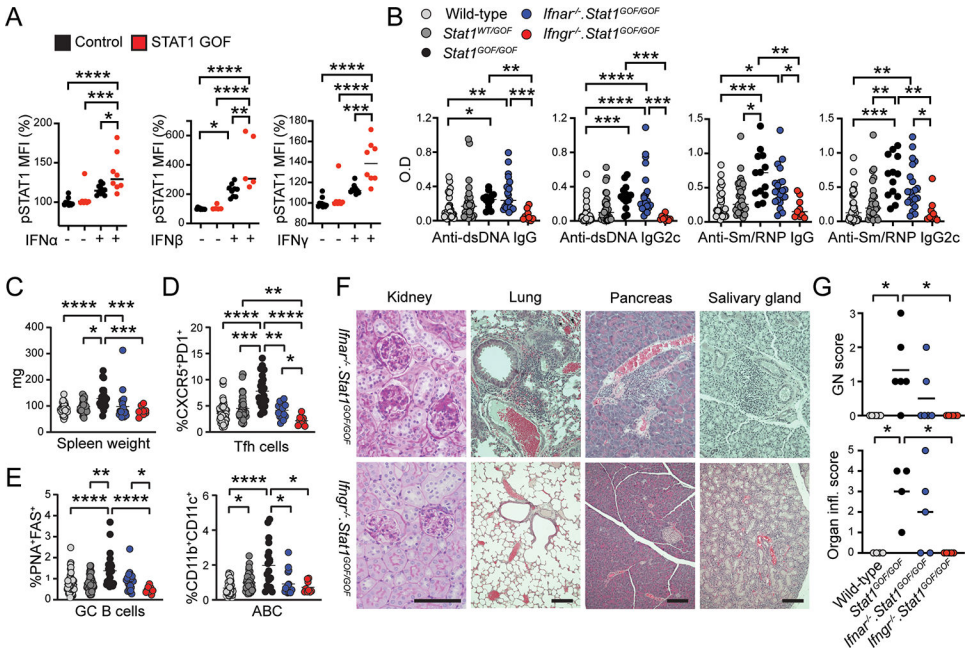

Figure 7: Dysregulated type 1 and type 2 IFN signals promote autoimmunity in STAT1 GOF syndrome

(A) Human T cells: $CD4^+$ T cell pSTAT1 MFI (normalized to unstimulated control) following IFN-α, IFN-β, or IFN-γ stimulation. Each data point indicates individual controls (black) and patients with STAT1 GOF syndrome (red). *, P<0.05; **, P<0.01; ***, P<0.001; ****, P<0.0001; by one-way ANOVA followed by Tukey multiple comparison test. N=1 human $CD4^+$ T cell in vitro stimulation. (B to G) Murine *Stat1*^{GOF} model: (B) Anti-dsDNA and anti-Sm/RNP IgG and IgG2c titers in indicated genotypes. (C to E) Spleen weight (C), Percentage of $PD1^+CXCR5^+$ Tfh cells (D), percentage of PNA^+FAS^+ GC B cells, and percentage of $CD11b^+CD11c^+$ ABCs (E) in indicated mice. (F) Representative images showing hematoxylin and eosin (H&E) staining of indicated tissues from *Ifnar*$^{-/-}$.*Stat1*$^{GOF/GOF}$ and *Ifngr*$^{-/-}$.*Stat1*$^{GOF/GOF}$ animals. Bars equal 100μm. (G) Composite score of glomerulonephritis (GN, upper) and organ inflammation (lower) in indicated genotypes. (B to G) Each dot represents an individual WT (light grey), *Stat1*$^{WT/GOF}$ (dark grey), *Stat1*$^{GOF/GOF}$ (black), *Ifnar*$^{-/-}$.*Stat1*$^{GOF/GOF}$ (blue), and *Ifngr*$^{-/-}$.*Stat1*$^{GOF/GOF}$ (red) animal. *, P<0.05; **, P<0.01; ***, P<0.001; ****, P<0.0001; by Kruskal-Wallis test with Dunn's multiple comparison test. Data compiled from 7 *Ifnar*$^{-/-}$.*Stat1*$^{GOF/GOF}$ and 3 *Ifngr*$^{-/-}$.*Stat1*$^{GOF/GOF}$ independent mouse cohorts.

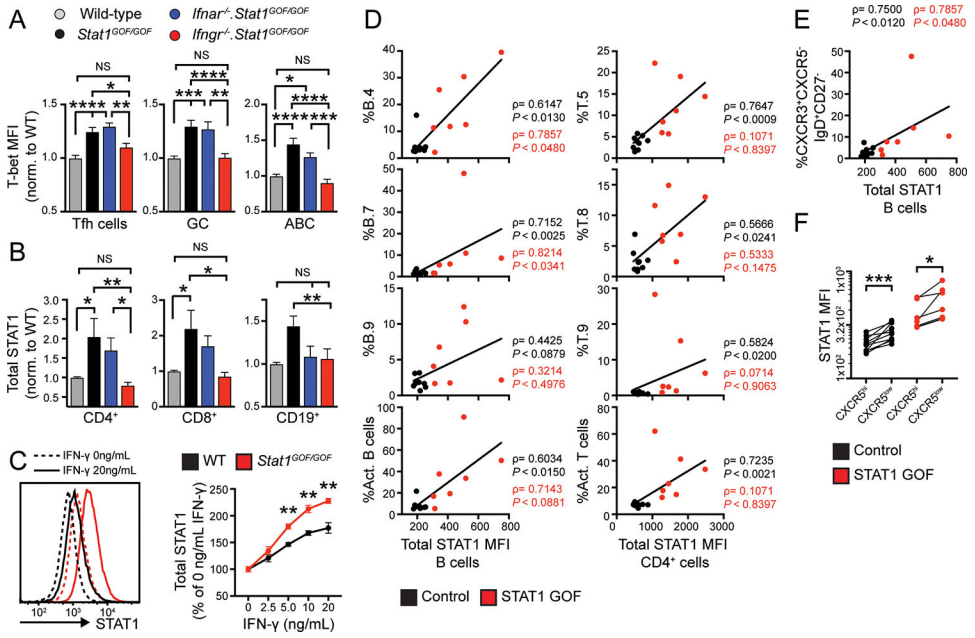

Figure 8: IFN-γ drives increased total STAT1 expression in STAT1 GOF syndrome:

(A to C) Murine *Stat1*^{GOF} model: (A) T-bet MFI (normalized to WT for each population) in WT (light grey), *Stat1*$^{WT/GOF}$ (dark grey), *Stat1*$^{GOF/GOF}$ (black), *Ifnar*$^{-/-}$.*Stat1*$^{GOF/GOF}$ (blue), and *Ifngr*$^{-/-}$.*Stat1*$^{GOF/GOF}$ (red) mice. (B) Total STAT1 abundance (normalized to WT for each population) in indicated genotypes. (C) WT and *Stat1*$^{GOF/GOF}$ B cells were cultured for 4 days on 40LB feeder cells [expressing CD40 ligand (CD40L) and B-cell activating factor (BAFF)] plus indicated concentrations of IFN-γ. Left panel: Histograms of total STAT1 expression assessed by flow cytometry in WT (black) and *Stat1*$^{GOF/GOF}$ (red) B cells, treated with 0 ng/mL (dashed) or 20 ng/mL (solid) IFN-γ. Right panel: Relative total STAT1 concentrations (normalized to 0 ng/mL IFN-γ condition for each genotype) in WT (black) and *Stat1*$^{GOF/GOF}$ (red) B cells. (A to C) *, P<0.05; **, P<0.01; ***, P<0.001; ****, P<0.0001; ns, not significant; by one-way ANOVA followed by Tukey multiple comparison test (A), by Kruskal-Wallis test with Dunn's multiple comparison test (B), and by unpaired Student *t* test (C). Representative of ≥2 independent experiments. (D to F) Human STAT1 GOF syndrome: (D) Spearman correlation of activated B cell (left) and CD4^{+} T cell (right) phenograph clusters versus total STAT1 concentrations in total B and CD4^{+} T cells, respectively. (E) Spearman correlation of IgD^{+}CD27^{-}CXCR5^{lo}CXCR3^{+} B cells versus total B cell STAT1. (F) STAT1 MFI in CXCR5^{hi} versus CXCR5^{lo} B cells from controls (black) and patients with STAT1 GOF syndrome (red). (D to F) Each data point indicates an individual healthy control (black) or patient with STAT1 GOF syndrome (red). Spearman correlation statistics are reported for combined population (black) and patients with STAT1 GOF syndrome alone (red). *, P<0.05; ***, P<0.001; by paired *t* test (F). N=1 CyTOF experiment.